



STRAIN AGEING IN ALPHA-TITANIUM

A. S. PEARCE

B. Applied Science (Adel)

A thesis submitted for the degree of Master of Applied Science in July 1973. The investigation was carried out in the Materials Science Group, Chemical Engineering Department, University of Adelaide.

TABLE OF CONTENTS

SUMMARY	1
DECLARATION	3
ACKNOWLEDGEMENTS	4
1. INTRODUCTION	5
1.1 Strain ageing mechanisms	8
1.2 Slip systems in zirconium and titanium	13
1.3 Present work	15
2. EXPERIMENTAL	16
3. RESULTS	24
3.1 Mechanical tests	24
3.2 Electron microscopy	40
3.3 Burgers vector analyses	46
4. DISCUSSION	47
5. CONCLUSIONS	53
BIBLIOGRAPHY	56

APPENDIX I: Preparation of 3mm disk electron microscopy
foils at subzero temperatures.

APPENDIX II: Automatic plotting of stereographic
projections.

APPENDIX III: Analysis of burgers vectors in Ti.

DECLARATION

This thesis contains no material which has been accepted for the award of any other degree or diploma in any university, and to the best of the author's knowledge and belief the thesis contains no previously published material or that written by any other person except where due reference is made or common knowledge is assumed.

A. S. PEARCE

ACKNOWLEDGEMENTS

The author wishes to thank Professor D. R. Miller, his supervisor, for his help during the work.

Particular thanks are also due to Mr. G. Wood for his critical appraisal at various stages and to Mr. B. Ide for his assistance in the design and maintenance of equipment and the preparation of specimens.

1. INTRODUCTION

Titanium and its alloys are gaining ever increasing importance as structural materials, especially in the aerospace industry. It is important therefore to have a thorough understanding of the behaviour of these materials through their service temperature range - up to 600°C. (Antony, 1965)

Many workers have observed anomalous behaviour in this temperature range. Rosi and Perkins (1953) in experiments on fine grained, commercial purity titanium observed discontinuous yield points on initial strain in the range 100° to 300°C and serrated yielding in the range 450° to 650°C.

Churchman (1955) using titanium single crystals containing 0.01 wt% oxygen observed no discontinuous yield point on initial strain. Specimens containing 0.1 wt% oxygen, however, did exhibit an initial yield point. If these specimens were immediately restrained a smooth continuous stress/strain curve resulted.

Annealing at 180°C for two hours was sufficient to reintroduce a discontinuity on restraining. Polycrystalline specimens of 99.35% purity and 25 grains/mm² grain size exhibited a discontinuous yield point at test

temperatures greater than 90°C .

Santhanam and Reed-Hill (1970) using commercial purity titanium of 16 microns grain size found evidence of dynamic strain ageing manifested as a work hardening peak in the temperature range 225° to 325°C . Santhanam et al (1970), working with the same material as the above, observed what they described as "non-ideal" behaviour of transients during strain-rate-change experiments in the range 300° to 400°C .

Turner and Roberts (1968) in experiments on commercial purity titanium - grain size 1000 to 1500 grains/ mm^2 - reported discontinuous yielding in the temperature range 100° to 450°C . They also found Luder's bands in the range 400° to 450°C .

Jones and Conrad (1969) carried out a series of room temperature experiments on both commercial purity and iodide refined titanium with grain sizes ranging from 0.8 to 30 microns. Commercial purity alpha-titanium exhibited discontinuous yield points on initial strain irrespective of grain size, whereas in fine grained iodide titanium only yield plateaux (no yield drops) were obtained. Coarse grained specimens (28 microns) exhibited no yield phenomena at all on initial strain.

Garde et al (1972) again using commercial purity and iodide refined specimens, found similar results up to 500°C. In experiments on high purity titanium, Jones and Conrad (1968) described a strain hardening peak in the range 125° to 375°C.

Anomalously low creep rates in commercial purity titanium in the temperature range 200°C to 400°C have been reported by Cuff and Grant (1952) and Juster et al (1953). Other workers have also reported behaviour consistent with strain ageing (Baird, 1971).

From the above it is obvious that strain ageing plays an important role in the mechanical behaviour of alpha-titanium in its service temperature range. The yield point and other strain ageing effects described have been generally interpreted in terms of a relatively weak interaction between interstitials, particularly oxygen and nitrogen, and dislocations (Rosi and Perkins, 1953; Turner and Roberts, 1968; Baird, 1971). It has been shown however that the interaction between interstitials and dislocations is very weak; indeed it has been suggested that the hardening effect of interstitials arises from the necessity to force the solute atoms out of the path of the mobile dislocation core (Tyson, 1967, 1968). Diffusion studies of O and N in titanium have

shown good correlation with the activation energy of the above hardening process. Taking this into account with the fact that in high purity alpha-titanium some prior deformation is necessary to produce a yield discontinuity in other than fine grained specimens (Churchman 1955; Jones and Conrad, 1969), it would appear that dislocation-dislocation interactions may also be involved. It has been reported that there is a tendency for titanium to form cellular dislocation arrays, even when strained at room temperature (Jones and Conrad, 1969). Since in such a substructure there is likely to be significant dislocation-dislocation interaction, investigations were conducted to determine if these interactions might play a role in the observed strain ageing phenomena.

1.1 STRAIN AGEING MECHANISMS

As has been shown elsewhere (Partridge, 1967; Tyson, 1968), there exist extensive similarities between the physical and mechanical properties of titanium and zirconium. Indeed Tyson (1968) in investigations into the effect of interstitials on the mechanical properties of titanium called heavily on the data for interstitial hardening in zirconium. In this investigation also an attempt to explain the behaviour of titanium will be

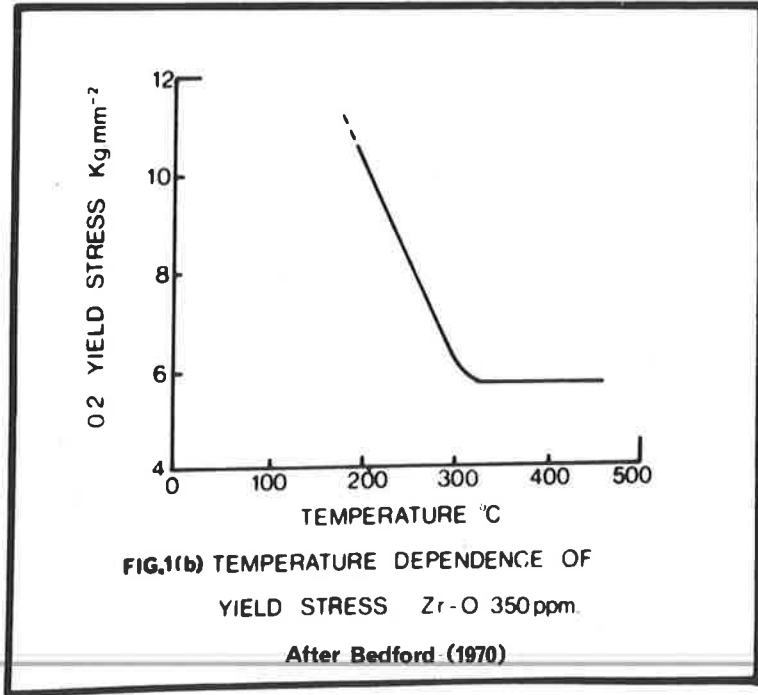
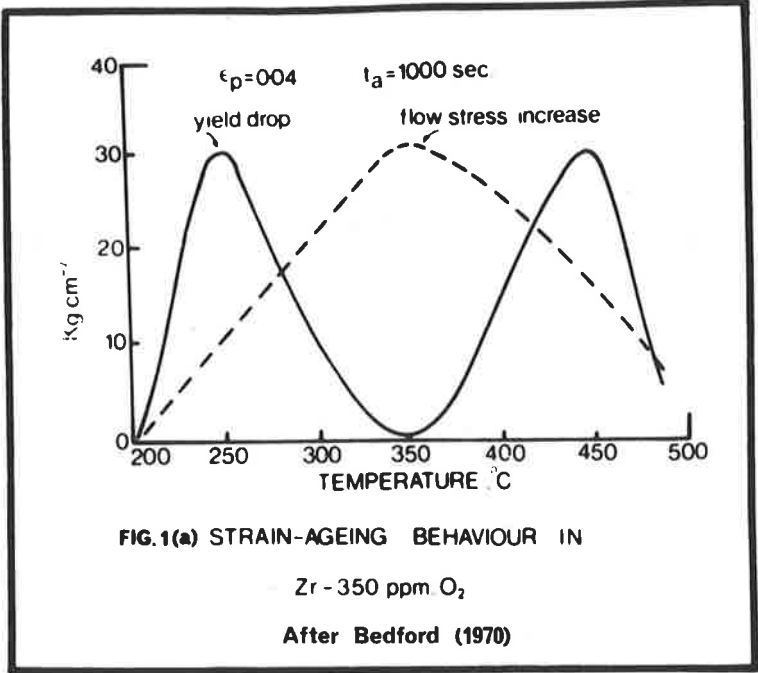
made in the light of results obtained with zirconium.

Many workers have reported discontinuous yielding in alpha-zirconium (Treco, 1953; Keeler, 1955; Reed-Hill et al, 1969; Ramaswami and Craig, 1967; Bedford, 1970). These phenomena were generally observed over the temperature range 200° to 400° C. The nature of the yielding behaviour and its thermal dependence are shown in figures 1(a) and 1(b) respectively.

Similarly, anomalies have been observed over this same temperature range in the creep behaviour of zirconium and its alloys (Holmes, 1964; Fidleris, 1968; Rotsey and Snowden, 1971).

Although discontinuous yield points have been reported for alpha-zirconium in the temperature range 200° to 400° C, one of the characteristics of the better known Fe/C or Fe/N systems, namely the occurrence of a sharp initial yield point which reappears after ageing, is not observed with the close packed hexagonal metals and alloys. This suggests a significant difference may exist between the strain ageing mechanisms in the Fe alloys and the c.p.h. ones.

Rotsey (1970) and Bedford (1970) have suggested



that a discontinuous yield point in zirconium occurs only in specimens in which straining, ageing and re-straining are all carried out at a temperature in the range 200° to 400°C . From transmission electron microscopy studies of thin foils treated in this way, Bedford reported that specimens strained and aged in the strain ageing temperature range were characterized by the presence of a well defined cellular substructure. The cell walls consisted of dense dislocation tangles while the cell interiors were virtually devoid of "free" dislocations.

Specimens strained less than 10% at room temperature or comparable strains at temperatures below the strain ageing range did not contain these well defined cells. Those strained at temperatures above 400°C , while exhibiting a cellular substructure, contained many free dislocations in the cell interiors. Consequent upon the findings of Bedford (1970) and his co-workers (Bedford et al, 1972) the following mechanism was suggested.

During initial strain in the temperature range 200° to 350°C dense dislocation tangles are formed resulting in a cellular substructure. As ageing proceeds these cell walls become more firmly established; also interstitial

atoms (oxygen) diffuse to the dislocation tangles further stabilizing the structure. Being a long range three-dimensional structure the dislocations are strongly locked in the cell walls. On restraining the specimens, the dislocations remain locked: when the upper yield point is reached new sources come into operation resulting in a sharp yield point.

Bedford explained the relatively narrow temperature range over which strain ageing is observed as follows. Specimens strained below 200°C did not exhibit a cellular substructure. Fuller (1971), using internal friction techniques, showed that at these temperatures oxygen has a jump time of greater than 10000 seconds. Therefore effective atmospheres do not form. At temperatures greater than 400°C free dislocations abound in the cell interiors so dislocation-dislocation interaction locking is much diminished. Also at these temperatures oxygen atoms have a jump time of less than 0.1 seconds, therefore while oxygen atoms readily diffuse to the dislocation cores, the dislocations are easily unpinned by thermal fluctuations. In both cases the criteria for discontinuous yielding are not met.

More recent work by Wood (1973) has necessitated some modification to the above hypothesis. Wood has found

that specimens strained at room temperature will subsequently exhibit a discontinuous yield point if they are aged and restrained in the strain ageing temperature range. Fuller (1971) showed that during ageing the mean free dislocation length decreased and he interpreted this in terms of a decrease in dislocation density and an increase in pinning points. Stress relaxation studies (Wood, 1973) further demonstrated considerable dislocation motion during ageing. Since dislocation rearrangement occurs during ageing, and since Wood was able to demonstrate strain ageing effects in specimens which did not develop cells on initial strain, it is conceivable that some cell formation occurs during ageing.

1.2 SLIP SYSTEMS IN ZIRCONIUM AND TITANIUM

In view of the similarity of these two metals one would expect them to have the same slip systems operating during deformation. The respective slip systems are shown in Table I. Williams and Blackburn (1968) have reported dislocations with $\langle 1\bar{2}3 \rangle$ type burgers vectors in titanium, although Bedford (1970) has cast some doubt on their observations.

This coincidence of deformation modes lends further

Table 1: Slip Systems in α -Ti and α -Zr ⁽¹⁾

Metal	Axial Ratio	Slip Systems	Remarks
Titanium	1.587	{0001}<11 $\bar{2}$ 0>	More common in impure metal ⁽³⁾
		{1 $\bar{1}$ 00}<11 $\bar{2}$ 0>	Principal slip system
		{1 $\bar{1}$ 01}<11 $\bar{2}$ 0>	All temperatures ⁽³⁾ In impure metal ⁽²⁾
Zirconium	1.593	{0001}<11 $\bar{2}$ 0>	Room temperature ⁽³⁾
		{1 $\bar{1}$ 00}<11 $\bar{2}$ 0>	Principal slip system
		{1 $\bar{1}$ 01}<11 $\bar{2}$ 0>	Low or high temp ⁽³⁾
		{11 $\bar{2}$ 2}<11 $\bar{2}$ 3>	Low or high temp ⁽³⁾

1. Bedford, A.J. Ph.D. thesis (1970) University of Adelaide.
2. Honeycombe, R.W. Deformation of Metal Crystals.
3. Yoo, M.H. and Wei, C.I. : J. App. Phys., 38, (1967), 4317

weight to the proposal that the strain ageing mechanism postulated for alpha-zirconium may well be operative in alpha-titanium.

1.3 PRESENT WORK

The present work was undertaken to determine if the above proposal - that the strain ageing mechanism postulated by Bedford (1970) is operative in both zirconium and titanium - is in fact a valid one. While making this comparison the following should be borne in mind. Although these two materials have very similar axial ratios - titanium: 1.5873; zirconium: 1.593 (Partridge, 1968) - there is a 10% difference in the size of the octahedral holes (titanium having the smaller) which are the interstitial sites (Tyson, 1967; Churchman, 1955).

Although it was shown earlier that interstitial-dislocation interactions are not solely responsible for the strain ageing effects observed, nonetheless they do have some influence on properties. It is to be expected therefore that while titanium and zirconium should exhibit the same general behaviour, there would be some differences in detail.

2. EXPERIMENTAL

The material used was electrolytic titanium from the U.S. Bureau of Mines, with the nominal chemical analysis as shown in Table II. The desired quantity of the material, in granulated form, was first compressed into a biscuit and placed on the hearth of an arc melting furnace. The furnace was evacuated until the pressure was less than 10^{-3} mm Hg absolute, then flushed several times with dry argon. Melting was carried out under dry argon at 80 mm Hg absolute pressure. Any residual oxygen and nitrogen were removed by gettering with molten zirconium for at least 30 minutes prior to melting the titanium.

The titanium was melted at least three times to ensure complete fusion and homogeneity. The button thus obtained was rolled into a cigar shape amenable to further deformation by swaging. This slug was chemically polished** and then annealed under a dynamic vacuum of better than 10^{-5} torr at 750°C for 30 minutes prior to being cold swaged into a rod 5.72 mm in diameter. From

** Chemical polish: 7.5% HF, 46.25% HNO_3 , 46.25 H_2O

TABLE II: Nominal Analysis of the Material Used as
Supplied by the U.S. Bureau of Mines.

Oxygen	0.030%
Carbon	0.015%
Nitrogen	0.005%
Chlorine	0.15%

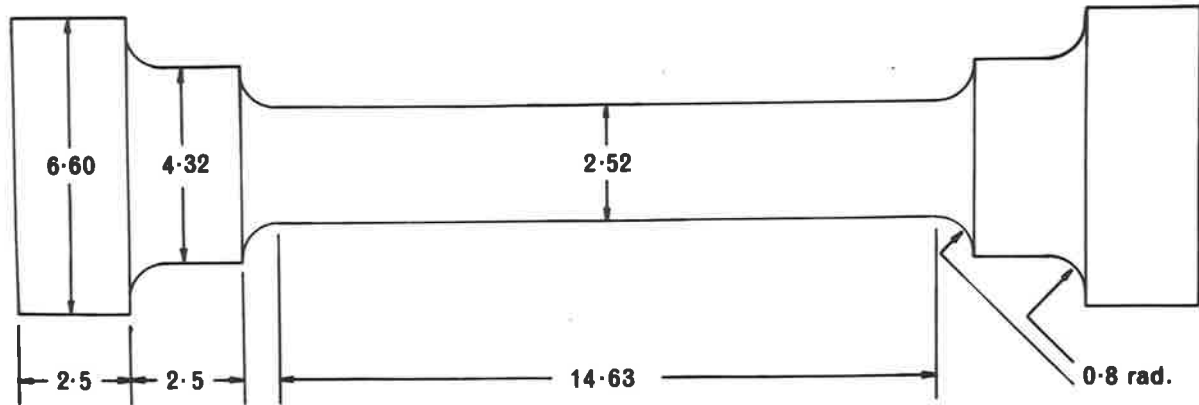
this rod round section tensile test pieces were machined with dimensions as shown in figure 2.

These specimens were chemically polished and annealed at 750°C for one hour, again under a dynamic vacuum of better than 10^{-5} torr, to produce a uniform structure of 35 micron grain size as determined by the linear intercept method (Gifkins, 1970). The final equivalent oxygen content, determined from hardness tests (Antony, 1965), was nominally 500 ppm (see figure 3).

Short time tensile tests from room temperature to 350°C were conducted on a hard tensile machine which has been described elsewhere (Wood, 1973). All tests were conducted in a dynamic vacuum of better than 10^{-5} torr, and at a strain rate of 4.17×10^{-4} per second.

The dislocation arrangements corresponding to various specimen treatments were determined by transmission electron microscopy using a Philips EM200 electron microscope. Transverse disk specimens were cut from the gauge length of each tensile test piece by spark machining. These disks were then chemically profiled using the method of Rice et al (1971), prior to the final perforation which was done electrolytically.

Figure 2: The tensile test specimen used in the present work.



dimensions in millimetres

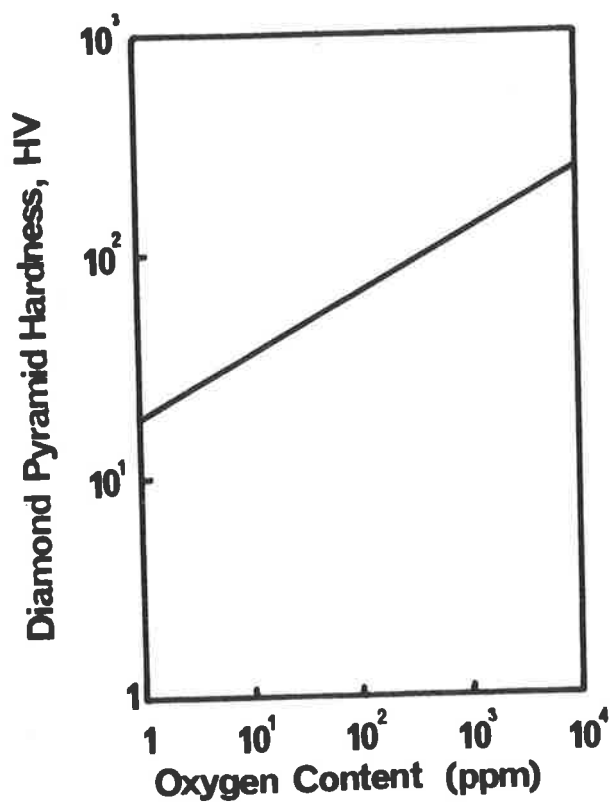


Figure 3: Increase in hardness with oxygen in titanium

After Antony (1965)

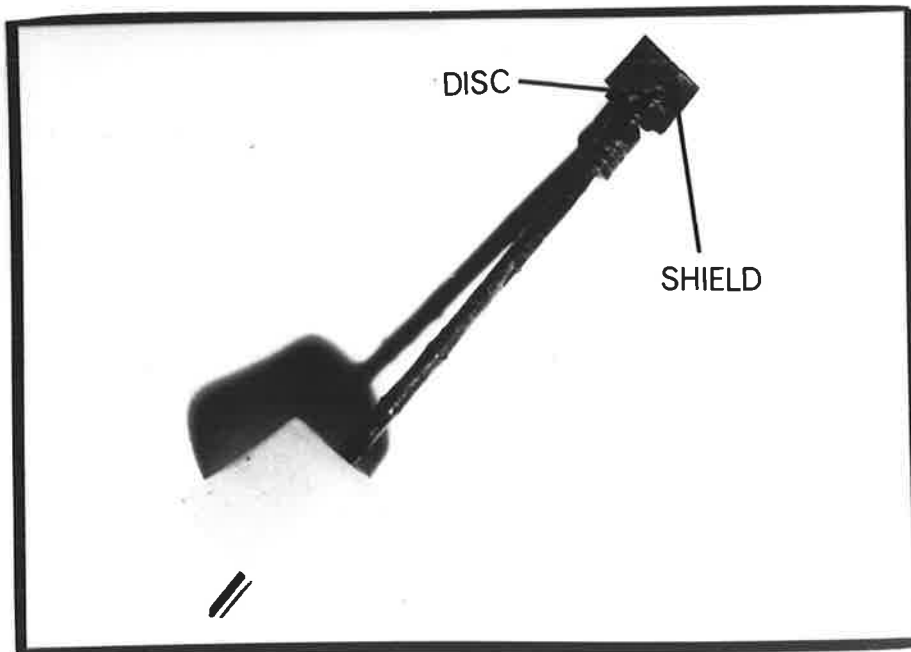
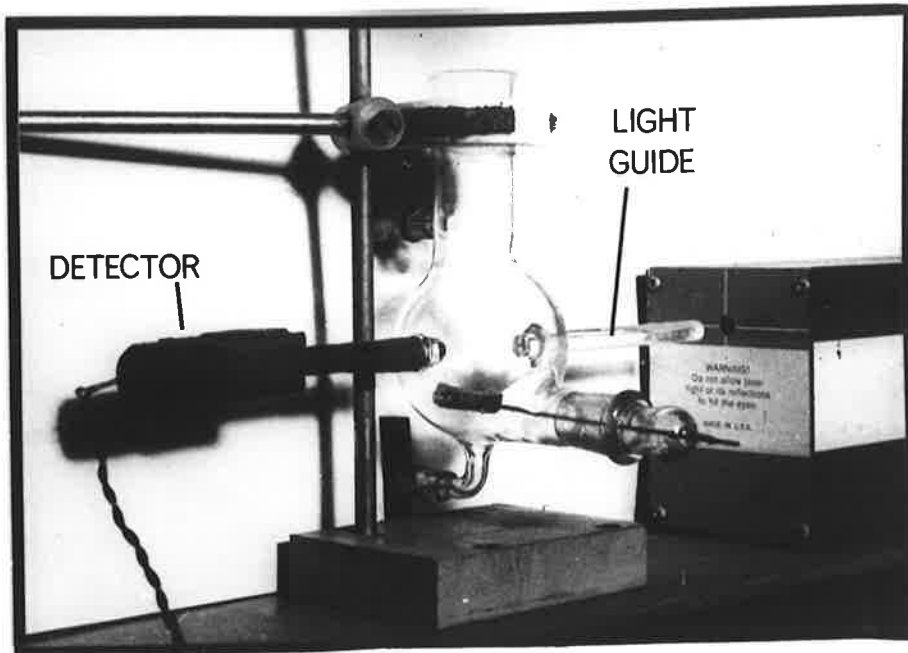
The final polish was automated using a modification of the method of Smialek and Mitchell (1971). These authors devised a technique whereby the specimen to be perforated was illuminated by a low power helium-neon laser beam. A photoelectric detector, placed on the opposite side of the specimen to the laser was connected into the power supply of the polishing cell in such a way as to switch off the polishing current at the moment of perforation. A laser was chosen as the light source as it provides an intense, well collimated beam. When the above method was used at the sub-zero temperatures required for the satisfactory polishing of titanium, it was found that thermal variation of the sensitivity of the photoelectric cell and the formation of frost in the light path rendered the technique useless. To overcome these difficulties a new polishing cell was designed.

This cell, shown in figure 4(a), consists of a pyrex glass polishing chamber into which two light guides (made of pyrex glass) and a stainless steel cathode have been embedded. In addition an inlet and outlet have been provided so that the electrolyte (6% perchloric acid, 36% n-Butanol, and 58% methanol, cooled to -60°C in a reservoir using a solid CO_2 /methanol freezing bath) is pumped through the cell and returned

Figure 4:

(a) The polishing cell (without masking)

(b) Specimen mounted in holder with shield



to the reservoir. The electrolyte is raised to the required temperature (-35°C) by passing it through a stainless steel tube wound with Kanthal and coupled to a Eurotherm stepless proportional controller. Temperature is measured with an iron/constantan thermocouple placed at the inlet to the polishing chamber.

Although the cell is shown with the shrouding removed it is in fact covered over with the exception of a window provided for alignment purposes, to prevent stray light from reaching the detector. Multiple reflections within the cell were eliminated by shielding the specimen as shown in figure 4(b).

To assist with the interpretation of electron micrographs, stereographic projections for titanium were prepared using a computer program derived from that published by Stokes et al (1968). (See Appendix II)

3. RESULTS

The tensile test pieces were given a 3% plastic pre-strain. The load was then reduced to that equivalent to half the 3% flow stress for 1000 seconds, after which the specimens were given a further 3% plastic strain. Each specimen was given the above treatment at a constant temperature within the range 17° to 350°C . Stress/strain curves are shown in figure 5; at no temperature was an initial yielding discontinuity observed.

At temperatures between 100° and 200°C an increase in flow stress was obtained on restraining. Specimens tested from this temperature up to 350°C (the highest test temperature used) exhibited discontinuous yield points after ageing. If figure 6, wherein the temperature variation of the lower yield stress is plotted, is compared with figure 1(b) it can be seen that titanium and zirconium behave in essentially the same manner in this regard.

Figure 7 shows the temperature dependence of the stress increment required to initiate deformation after ageing (the upper yield point) and that required to maintain deformation (the lower yield stress), both being

Figure 5: True stress/true strain curves at various temperatures

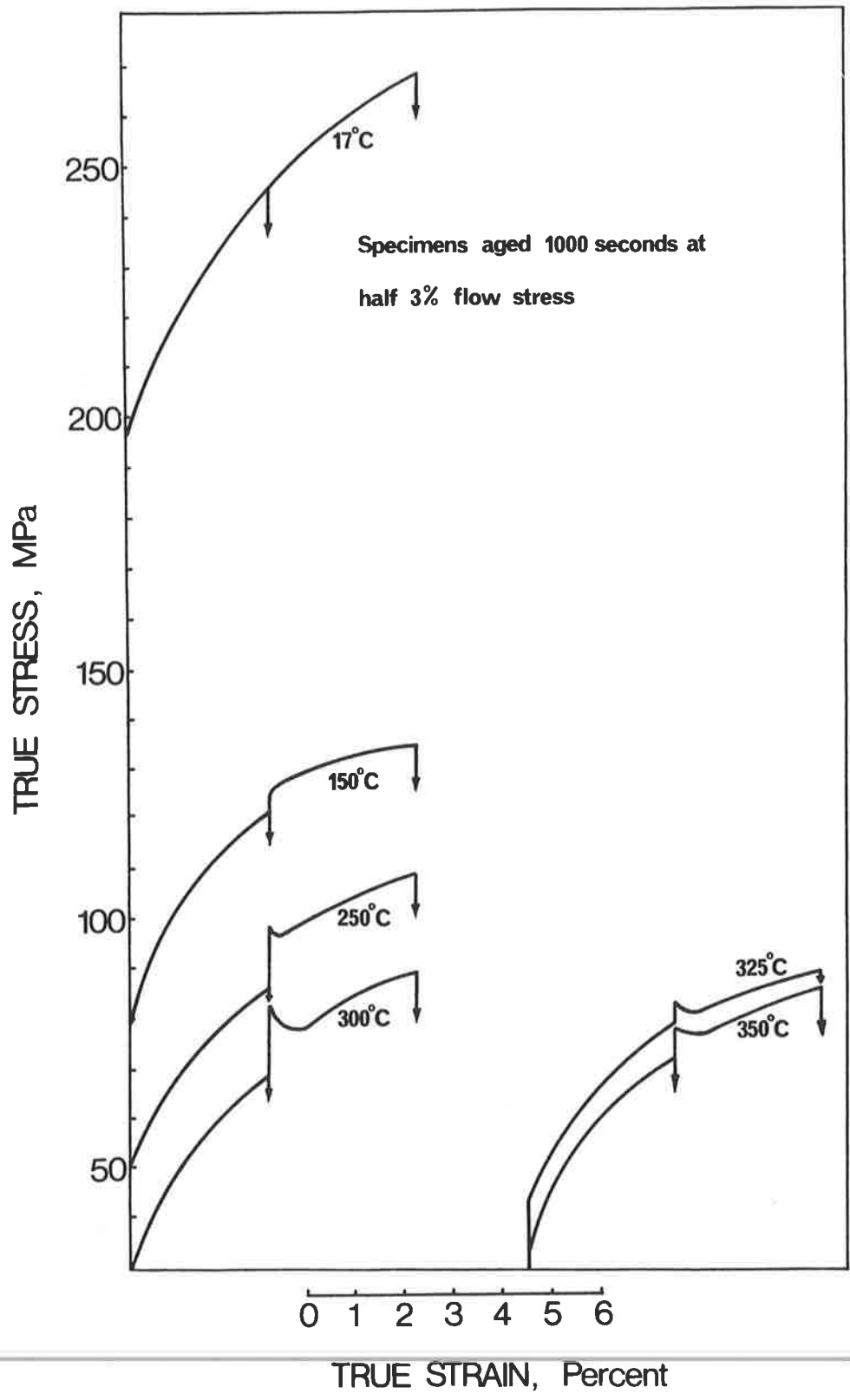


Figure 6: Variation of lower yield stress after ageing with temperature

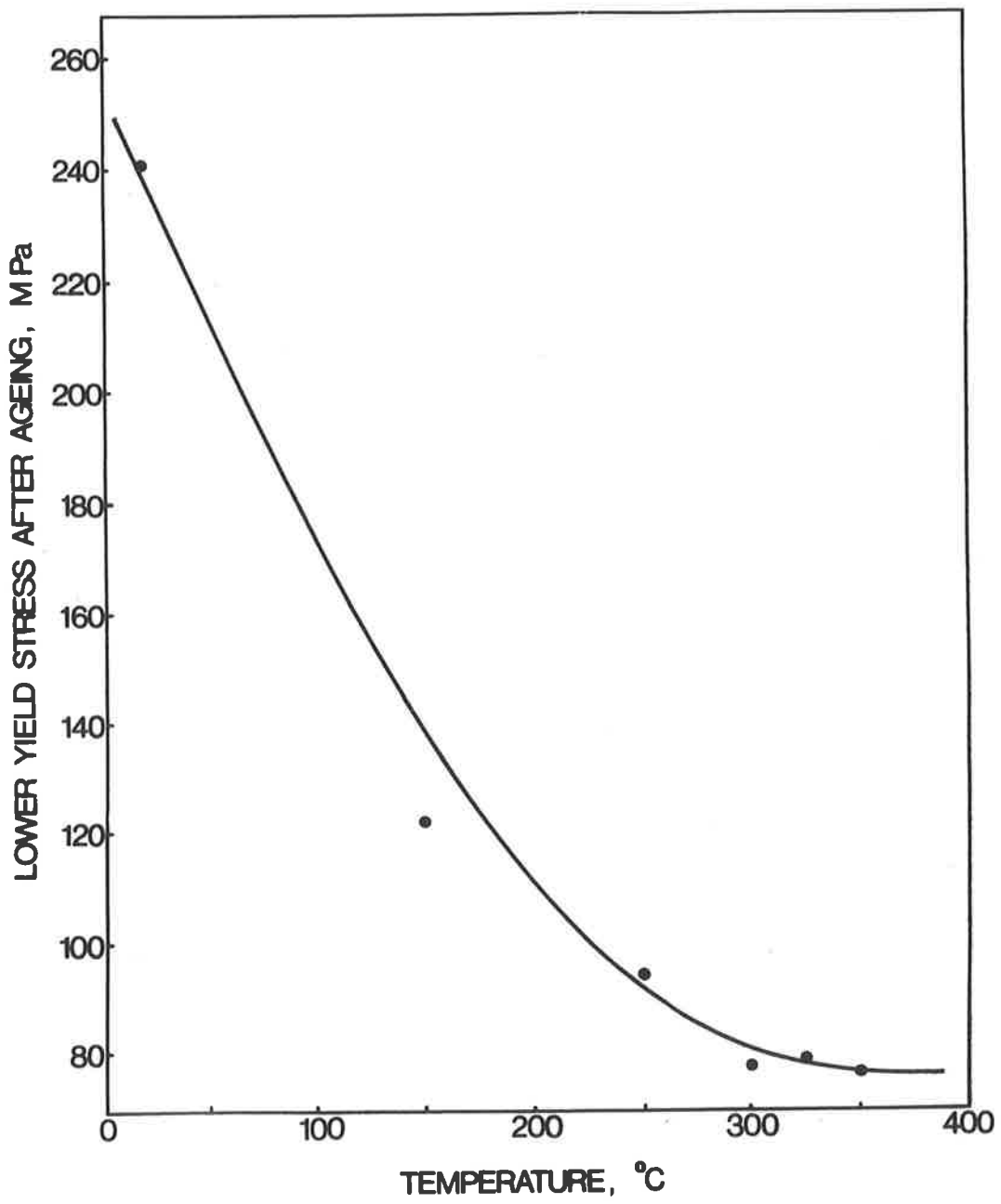


Figure 7: Variation of increase in strength after ageing with temperature. The parameters plotted are shown in figure 8.

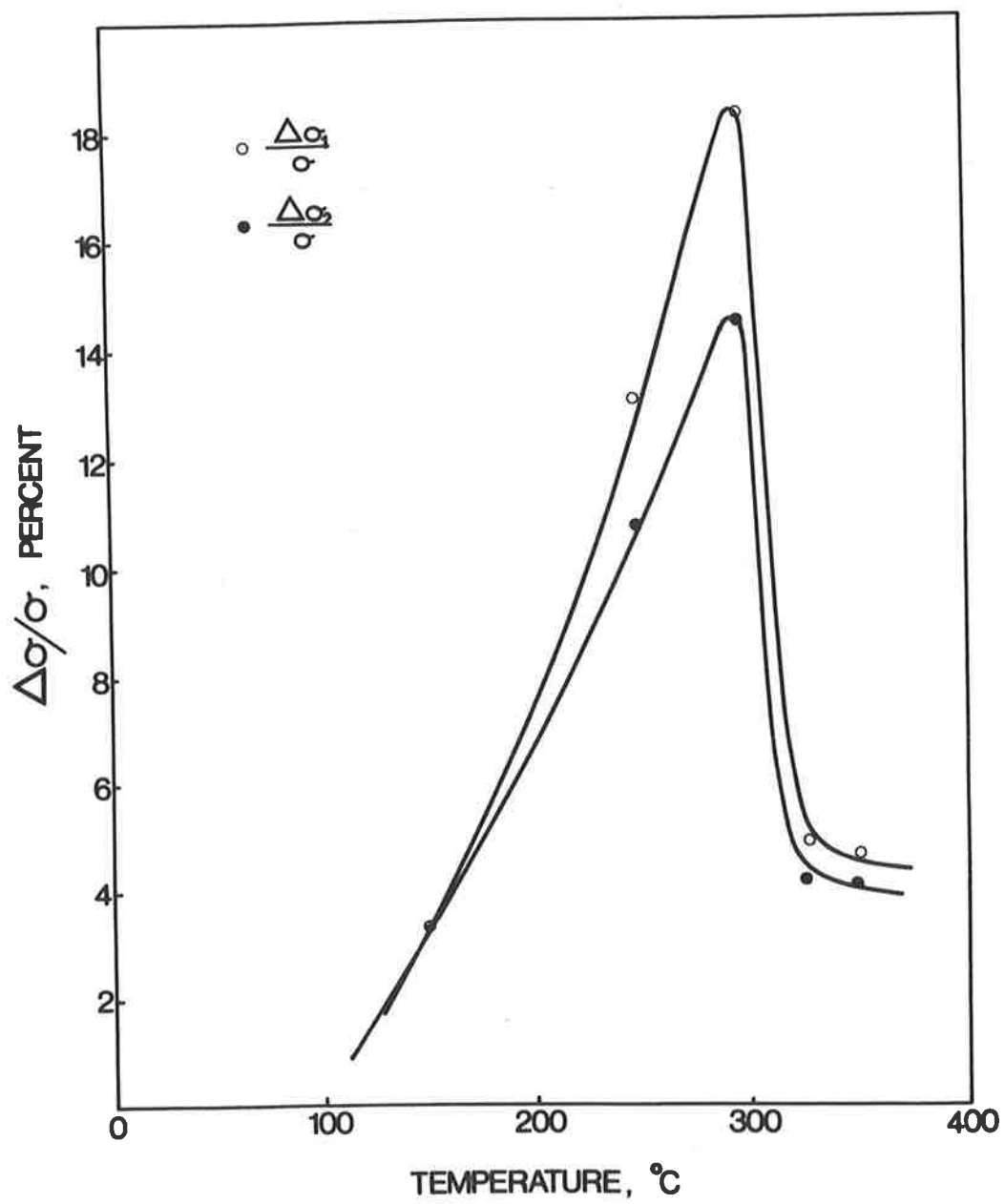
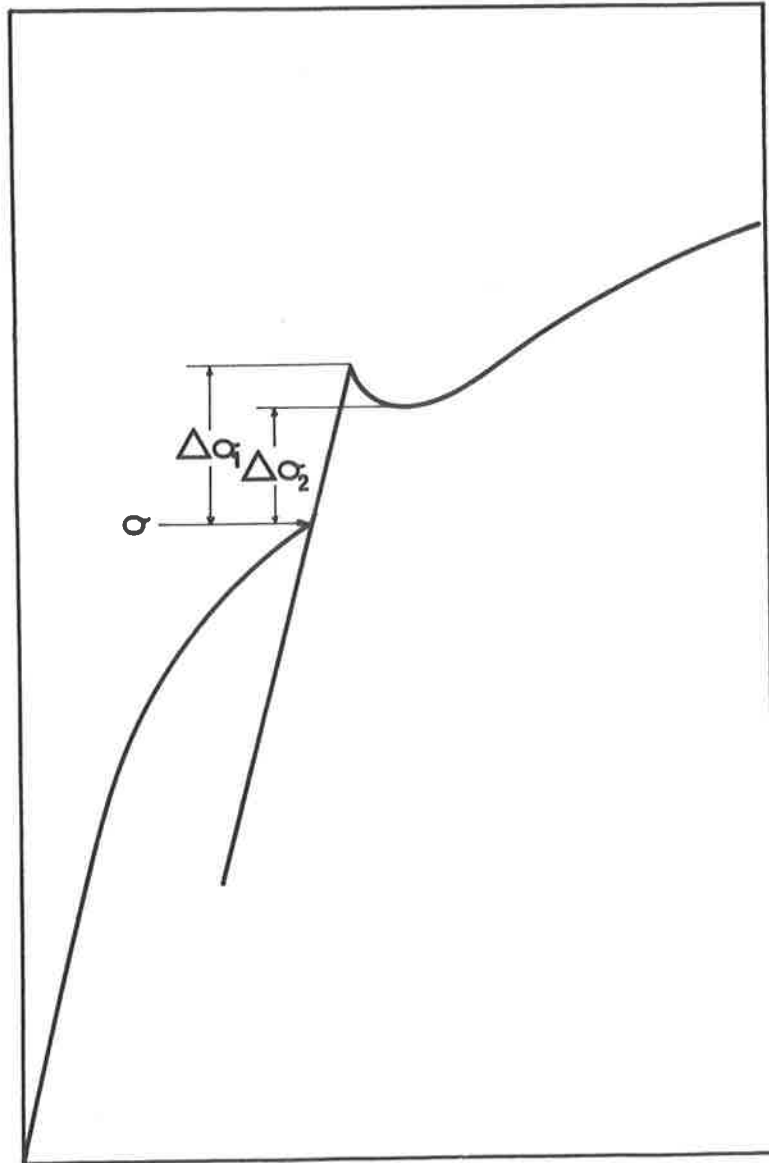


Figure 8: Definitions of the parameters plotted
in figure 7.

STRESS



STRAIN

expressed as a percentage of the 3% flow stress at that temperature. The actual parameters plotted are defined in figure 8. The preceding figures 5, 6, and 7 indicate that high purity titanium exhibits strain ageing phenomena in the range 100° to 350°C, with the effects being most pronounced at about 300°C.

Given the strain ageing mechanism of Bedford (1970) and assuming it is operative in titanium, then one would expect evidence of the presence of dynamic strain ageing since it is the interaction of dislocations during straining that is held to be responsible for the effects observed. One method of determining if dynamic strain ageing occurs is to study the temperature variation of the work hardening behaviour of the material under investigation. In the absence of dynamic strain ageing the work hardening rate would be expected to decrease with increasing temperature due to the decreasing thermal component of stress and the increasing operation of thermally activated dislocation sources. If dynamic strain ageing occurs however, deviation from this behaviour would be expected.

Ludwik (1909) suggested the following simplified power curve to describe tensile behaviour in the plastic range:

$$\sigma = \sigma_0 + k \cdot \epsilon^n \dots\dots\dots(i)$$

where n , the strain hardening exponent, is related to the work hardening behaviour of the material. Plotting the stress/strain curve on logarithmic co-ordinates should then yield a straight line of slope n . This was done for a series of test temperatures; the plots are shown in figure 9. The results thus obtained are in good agreement with those obtained with zone refined polycrystalline zirconium by Arunachalam et al (1972). The values of n , when plotted against temperature, show a distinct work hardening peak at 300°C (figure 10).

It has been suggested that a more realistic measure of work hardening would be the work hardening rate, $d\sigma/d\epsilon$, (Kelly, 1972) which is in fact the instantaneous slope of the stress/strain curve. From equation (i):

$$\begin{aligned} \frac{d\sigma}{d\epsilon} &= n \cdot k \cdot \epsilon^{(n-1)} \\ &= \frac{n \cdot k \cdot \epsilon^n}{\epsilon} \\ &= \frac{n(\sigma - \sigma_0)}{\epsilon} \dots\dots\dots(ii) \end{aligned}$$

The variation of $(d\sigma/d\epsilon)_{\epsilon = .03}$ with temperature is shown in figure 11; again a peak is observed in the strain ageing range.

Figure 9: $\log(\text{true stress})$ vs $\log(\text{true strain})$ at various temperatures

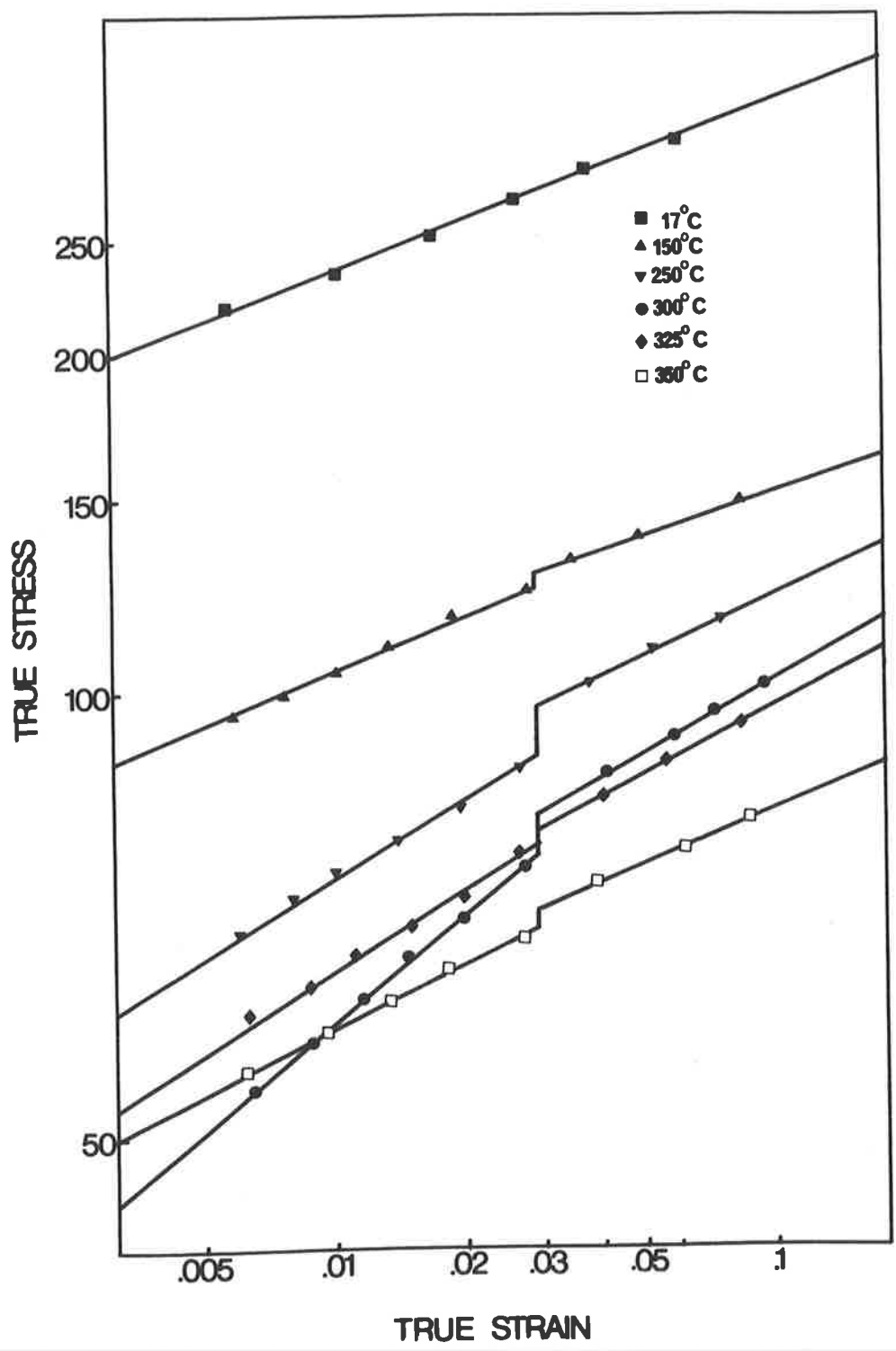


Figure 10: Thermal variation of the work hardening exponent, n

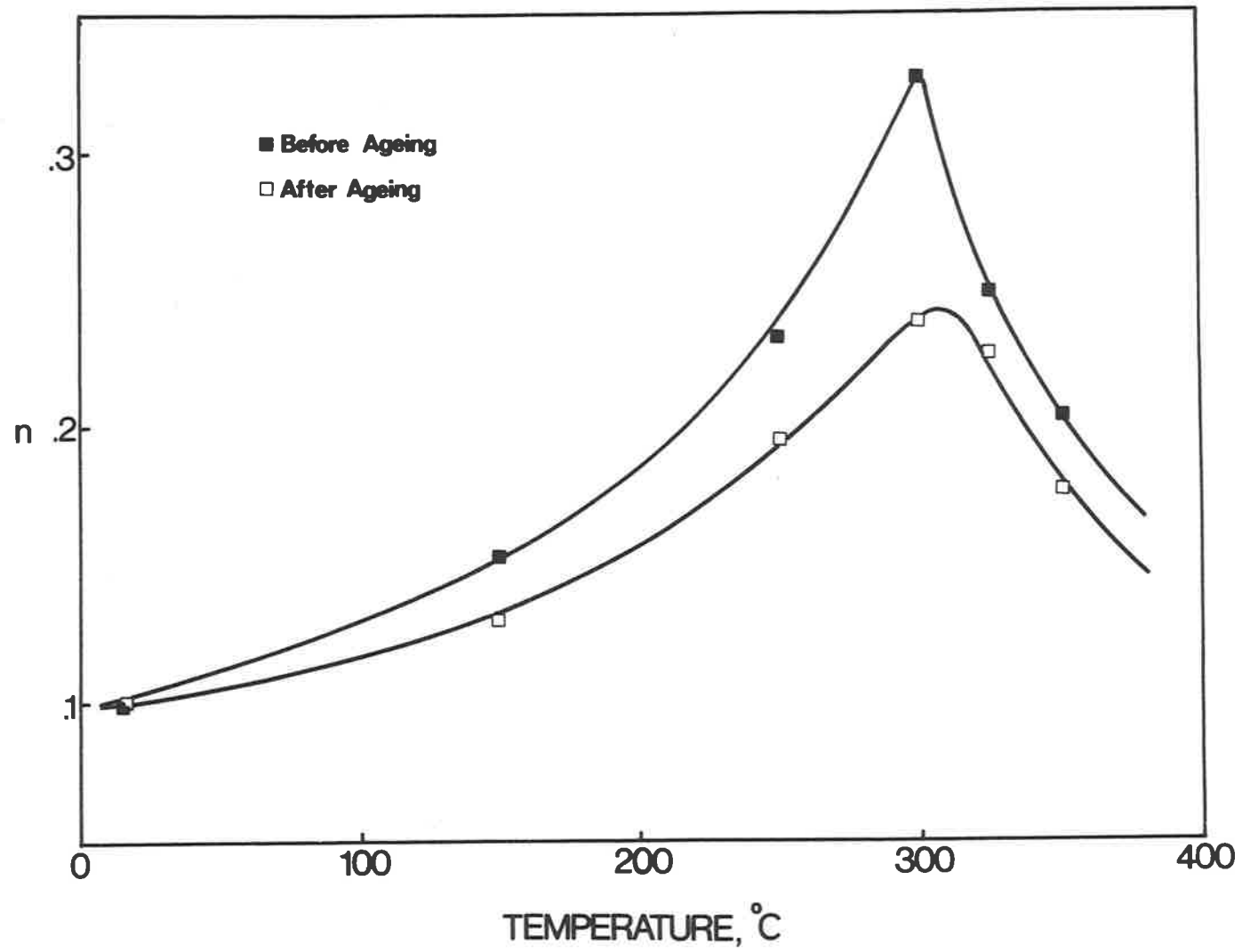
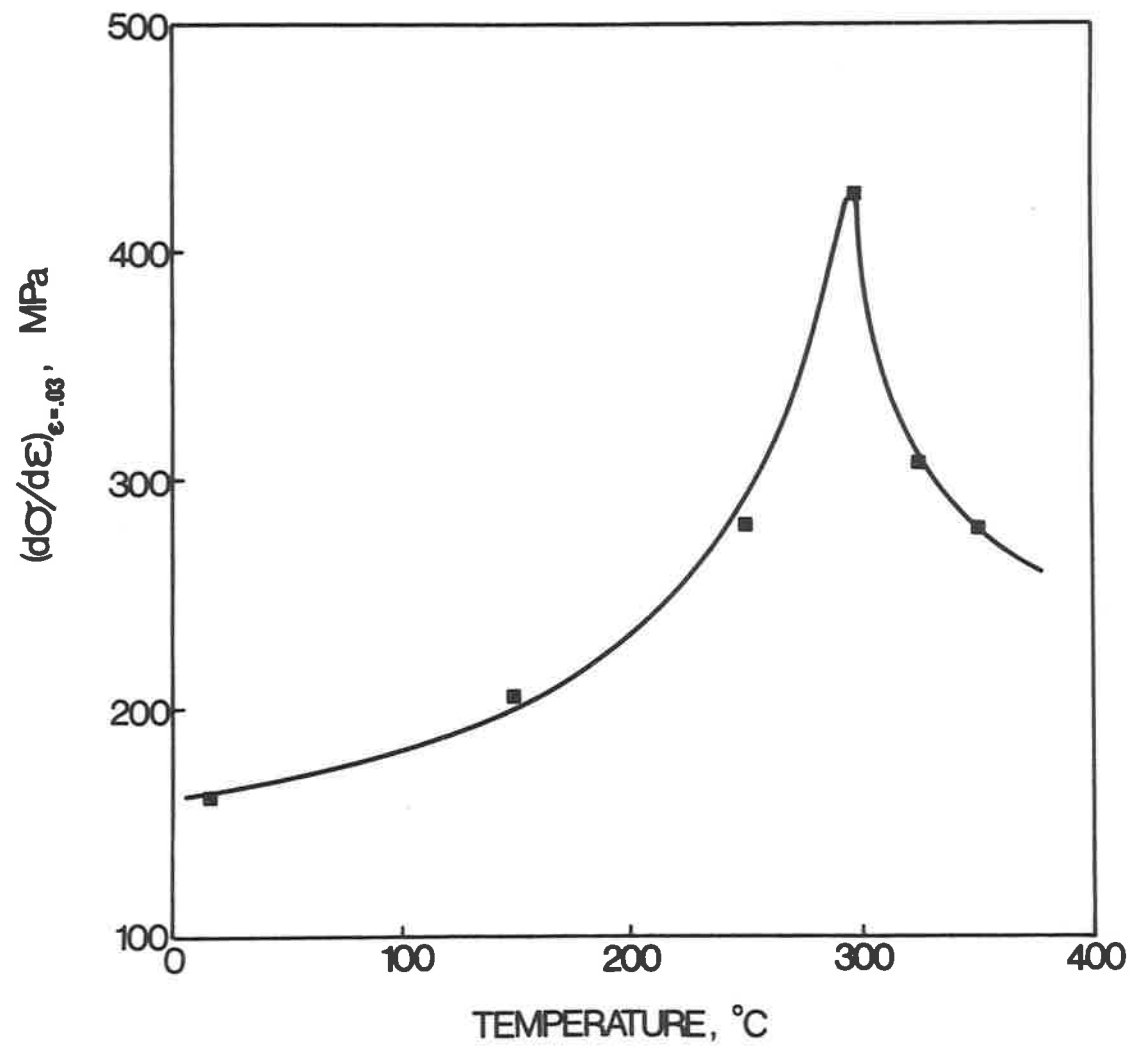


Figure 11: Thermal variation of the work hardening
rate, $(d\sigma/d\epsilon)_{\epsilon=.03}$



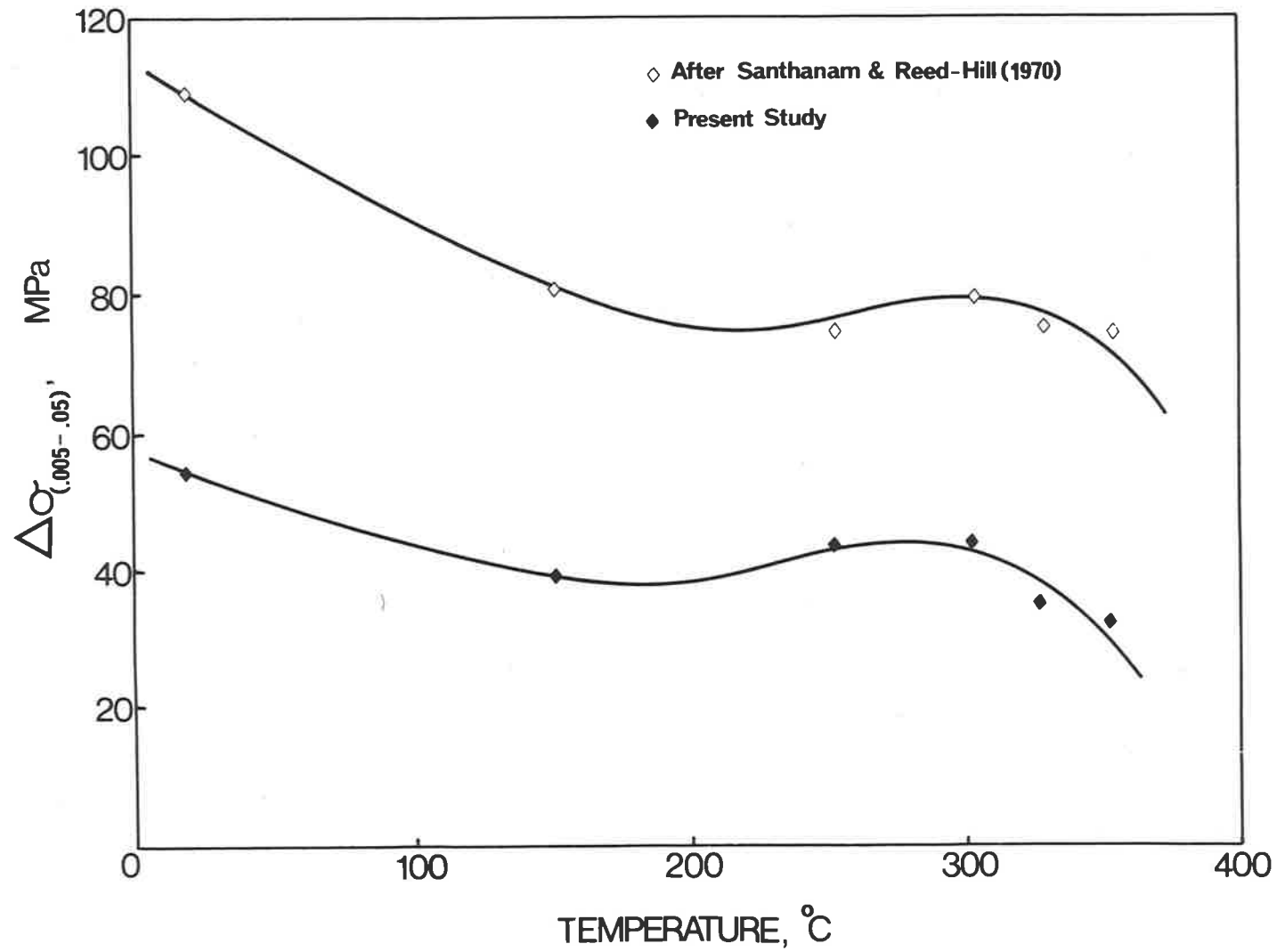
Santhanam and Reed-Hill (1970) have suggested that a better assessment of work hardening can be made by measuring the stress increment required to increase the plastic strain from 0.5% to 5.0%. This procedure has the advantage that it makes no assumptions about the shape of the stress/strain curve and the increment is not influenced by changes in the thermally activated flow stress component. Figure 12 shows $\Delta\sigma_{0.05,0.5}$ versus temperature; the data of Santhanam and Reed-Hill are included for comparison.

The stress increment at any given temperature is less for the higher purity material. The higher the purity the lower the dislocation density for a given strain (Kelly, 1972; Conrad et al, 1972), hence the lower the long range stress component and the less stress required to induce the strain.

All three methods indicate that dynamic strain ageing does occur in high purity titanium over the same temperature range as that over which discontinuous yield points are observed.

Referring again to figure 12, another significant observation can be made with regard to the shapes of the

Figure 12: $\Delta\sigma(.005 \rightarrow .05)$ vs temperature



two curves plotted. Both show an anomalous work hardening rate in the temperature range 150° to 350°C and more importantly the magnitude of the effect, as measured by the peak height relative to the background curve, is the same in each case. It has been shown that for a given strain, dislocation density increases with impurity content (Kelly, 1972; Conrad et al, 1972); since the internal stress component is directly related to dislocation density (Orlová et al, 1972; Kratchovil and Conrad, 1970; Conrad et al, 1972) the higher stress increment obtained for the commercial purity material is expected. If however, solute-dislocation interactions were solely responsible for the observed dynamic strain ageing effects, then considering the great disparity in solute content of the commercial purity and electro-refined materials, the noted similarity of the effect in the two materials would not be expected.

Since the only other mechanisms which might cause ageing are point defect (other than solute atoms)-dislocation and dislocation-dislocation interactions, the occurrence of dislocation cells over the same temperature range as that over which the anomalous work hardening behaviour is observed (§3.2) assumes a new significance. If it is hypothesised that dislocation-

dislocation interactions within these cells are involved in ageing (a reasonable proposal in view of the reported behaviour of zirconium ($\phi 1.1$)) then a modification of the stress relaxation behaviour in the strain ageing range would be expected.

Stress relaxation requires the movement of dislocations over many atomic distances. If dislocations become enmeshed in dense tangles during straining, stress relaxation should be severely inhibited. Qualitative comparisons of stress relaxation behaviour at various temperatures were made; the results obtained at room temperature and 300°C are shown in figure 13. A specimen relaxed at room temperature from the 3% flow stress exhibits exponential relaxation behaviour both initially and after reloading to the 3% flow stress level. This is in direct contrast to the results obtained at 300°C where initially there is only a very short period of exponential decay, followed by linear relaxation with a very low rate of load drop.

Tests were conducted to determine if static strain ageing occurred to a significant extent in high purity titanium. Specimens were strained 3% at room temperature, aged (under no stress) and restrained, both at 300°C .

Figure 13: Stress relaxation behaviour of titanium
at 17°C and 300°C

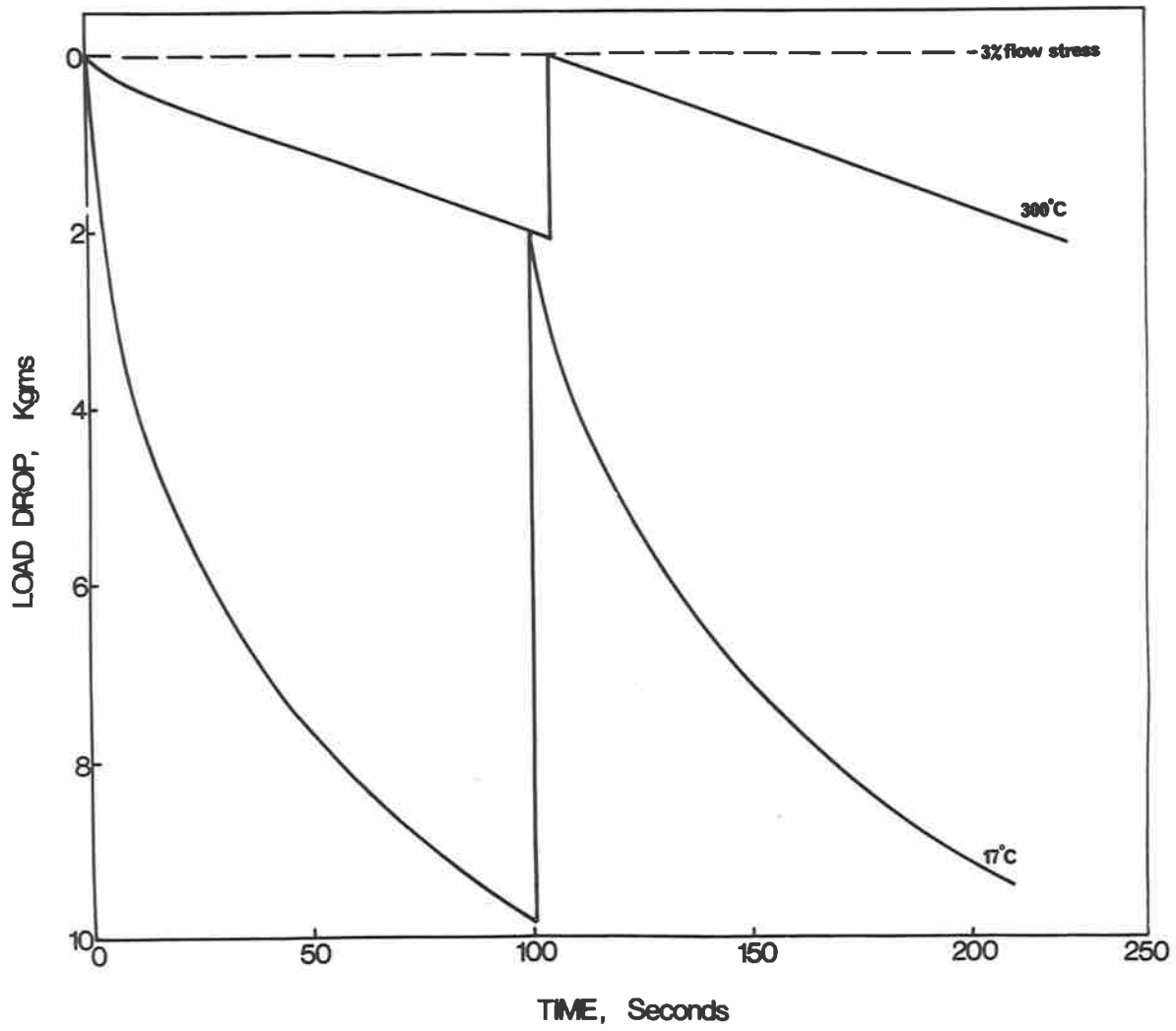
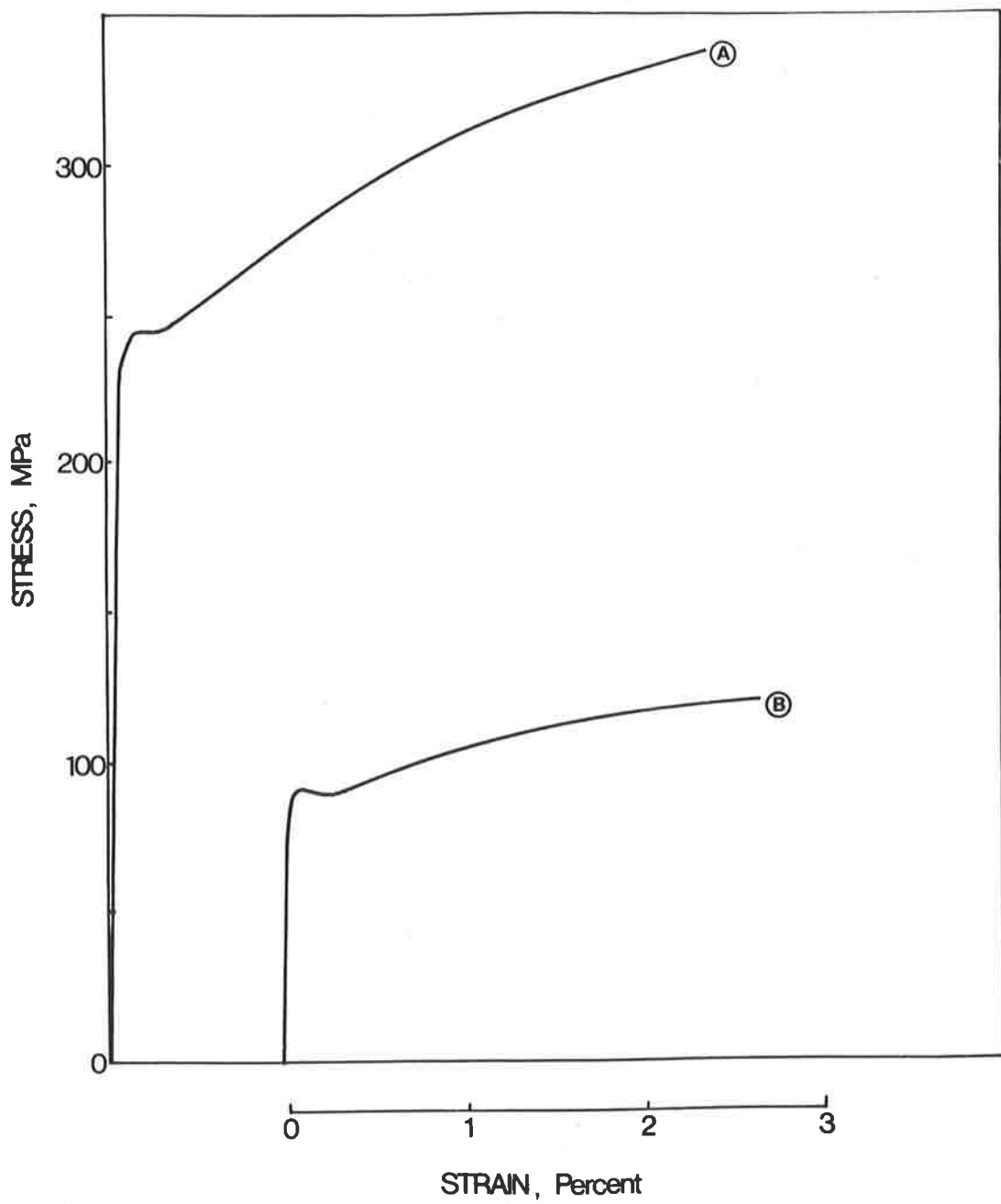


Figure 14: The effects of different ageing treatments on titanium.

Curve A: restrained at room temperature after 3% strain and ageing, both at 300°C.

Curve B: aged and restrained at 300°C after 3% room temperature strain.



The result is shown in figure 14 (curve B); a discontinuous yield point has been introduced, although the effect is not as pronounced as that obtained when the initial strain is conducted at 300°C.

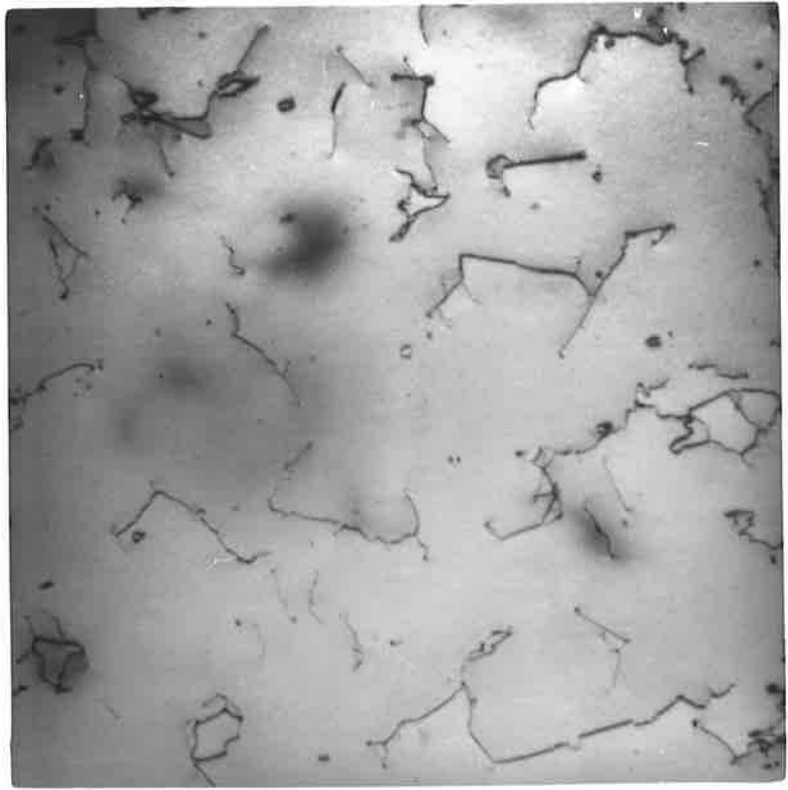
It was suggested earlier that the strain ageing behaviour of titanium should be similar to that of zirconium, but with some modification due to the differing elastic interaction energy of interstitials in the respective lattices. In titanium, where the misfit is greater, the interaction between interstitials and dislocations should be correspondingly greater. Bedford (1970) showed that the combined effects of dislocation-dislocation and interstitial-dislocation interactions were such that the ageing effects were masked when an aged specimen was restrained at room temperature. Titanium specimens which were strained and aged at 300°C and restrained at room temperature exhibited a yield plateau (figure 14, curve A) indicating stronger locking than is the case for zirconium.

3.2 ELECTRON MICROSCOPY

Specimens which had been given the annealing treatment described earlier exhibited a typical dislocation structure, with a low density, random distribution of

Figure 15: Dislocation structure in specimen
annealed at 750°C for one hour.

Magnification: 22000X






Figure 16: Dislocation structure developed after
3% strain at room temperature.

Magnification: 22000X

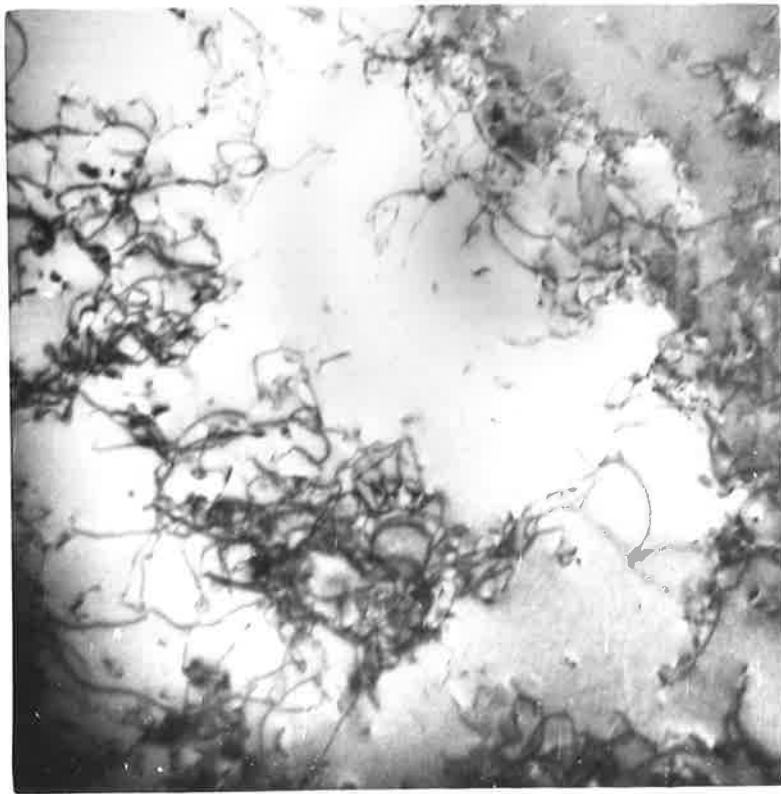


Figure 17: Cellular substructure developed after
3% strain at 250°C.

Magnification: 22000X

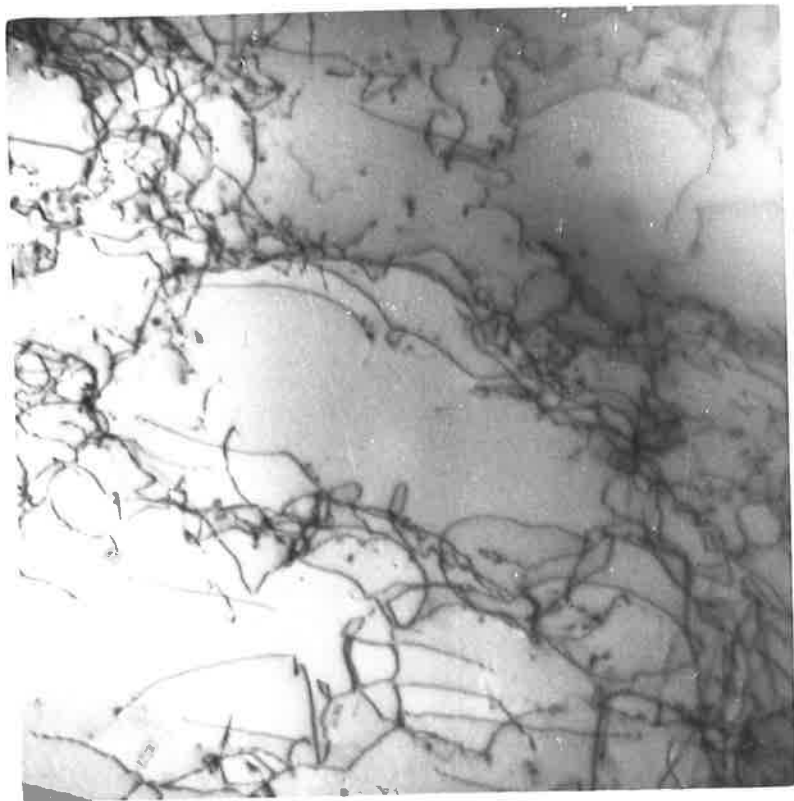


Figure 18: As for figure 17 except specimen
strained at 300°C.

Magnification: 22000X

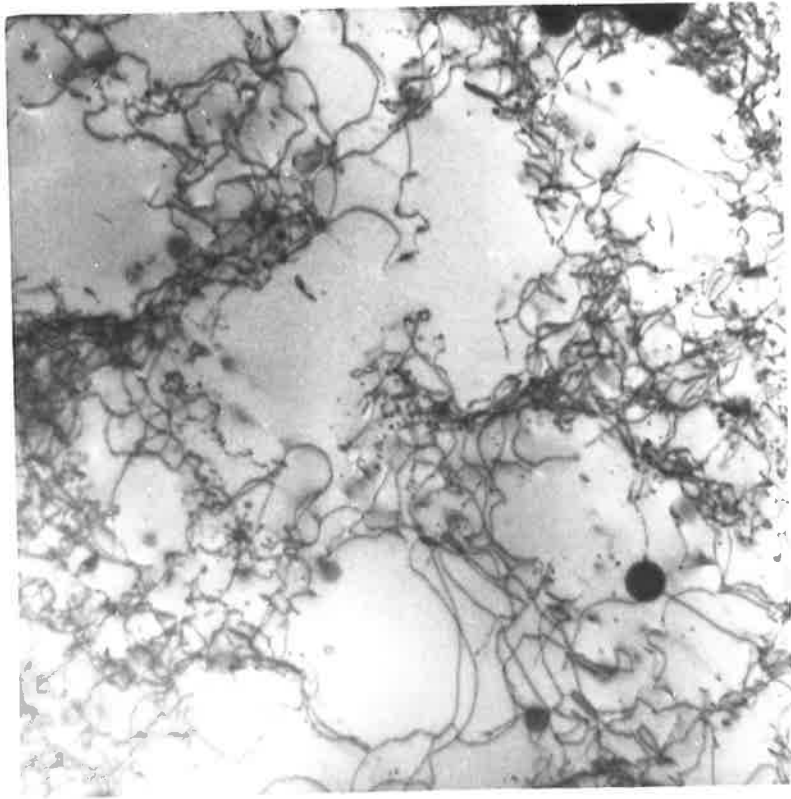
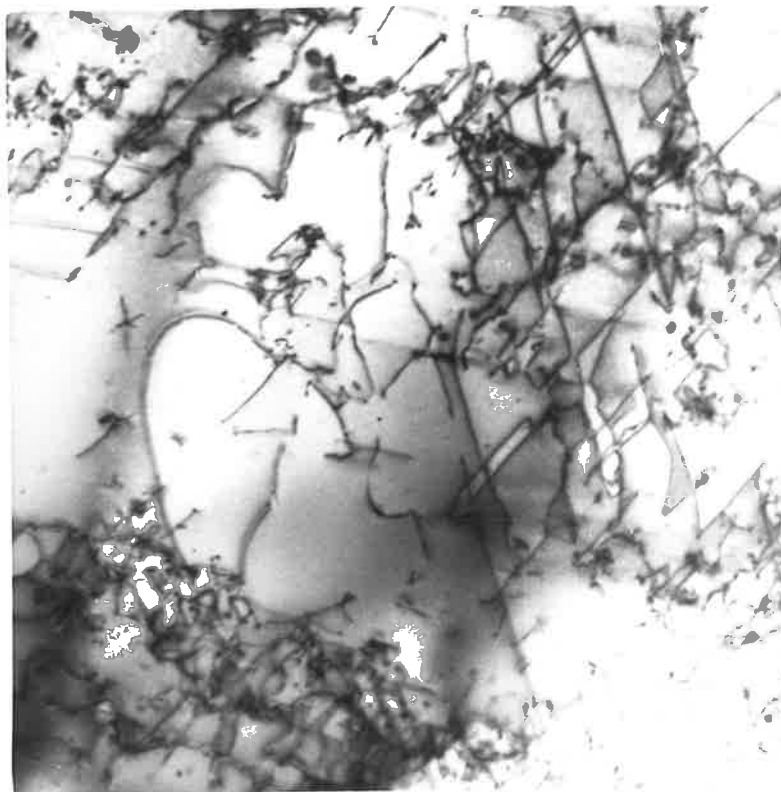


Figure 19: As for figure 17 except specimen
strained at 350°C.

Magnification: 22000X



dislocations (figure 15). Straining 3% at room temperature produced large, loosely defined, cellular arrays and many free dislocations in the cell interiors (figure 16). The same deformation at 250°C produces a cellular substructure, the walls of which contain heavily tangled dislocations and debris, with virtually no free dislocations (figure 17). Deformation at 300°C produces essentially the same structure (figure 18) as does straining at 350°C, although in this latter case more free dislocations are apparent in the cell interiors (figure 19).

3.3 BURGERS VECTOR ANALYSES.

In order to compare the slip systems operating, burgers vector determinations were conducted on specimens strained at different temperatures, using the technique of Bedford and Miller (1970). In all cases dislocations were found to have burgers vectors of the $\langle 11\bar{2}0 \rangle$ type. A typical analysis is given in Appendix III.

4. DISCUSSION

It is now generally agreed that for a discontinuous yield point to occur all dislocations present in the material must remain effectively locked until the onset of microstrain. At the upper yield stress there is a sudden multiplication of the number of mobile dislocations present.

Depending on the strength of the locking mechanism this multiplication may be caused by a few dislocations moving through the lattice at high speed and multiplying rapidly or, in the case of strongly pinned dislocations, new dislocations may be created at stress concentrations. These dislocations, again, multiply rapidly resulting in a yield drop.

Crussard (1963) proposed a mechanism, in actuality a combination of the Cottrell and dislocation-dynamics theories, in which it was considered that prior to a yield point occurring, a few sources will operate by a thermal activation process. These dislocations pile up against grain boundaries; the resulting stress concentrations eventually initiate slip in the neighbouring grains. Rapid dislocation multiplication follows giving

a yield drop.

Bedford (1970) interpreted his observations in alpha-zirconium, where dislocation tangles occurred more often in the vicinity of grain boundaries than in the grain interiors, as supporting the model of Crussard. The necessary statistical computations were not done in this work to enable a comparison of dislocation distributions to be made.

As was stated in the introduction, in zirconium a Cottrell locking mechanism acting alone has been discounted as being responsible for producing the strain ageing effects observed. Using the definition of Nabarro (1946) for lattice distortions resulting from the presence of solute atoms, the asymmetry ratio, $\epsilon_D(c)/\epsilon_D(a)$, for oxygen in zirconium has been found to be 1.2 (Hull and Conrad, 1967). Hence no hardening of the type described by Fleischer as being due to tetragonal strain fields is observed. In titanium the asymmetry ratio is 30 (Pearson, 1958) therefore Fleischer hardening will occur. Measurements of activation energy however, have shown that the interaction between dislocations and interstitials cannot be accounted for by this mechanism (Tyson, 1967). Further, Hull and Conrad (1967) have shown that in the case of

titanium the influence of interstitial content on short range internal stress is less pronounced than in zirconium. They have explained this in terms of the lattice distortions that result when an interstitial atom is placed in the respective lattices. While the lattice distortion in zirconium is less than in titanium, the former is virtually symmetrical (see above) whereas the latter occurs almost entirely in the "c" direction (Pearson, 1958); the strain in the "a" direction is therefore greater in zirconium than it is in titanium. This means that for prismatic slip the interaction between a mobile dislocation and an interstitial atom will be greater in zirconium than in titanium.

From the foregoing it can be seen that interstitial-dislocation interactions are not solely responsible for the ageing effects observed. The electron microscopy studies showed that the substructures concomitant with ageing were cellular dislocation arrays, a situation involving extensive dislocation-dislocation interaction. Further, the dynamic strain ageing studies revealed an ageing effect, the magnitude of which is apparently insensitive to the disparity in solute content that exists between iodide refined and commercial purity titanium. Stress relaxation experiments showed that only

very little stabilization of the structure developed during straining was necessary to greatly inhibit dislocation motion. It would appear therefore, that the dislocation-dislocation interactions resulting from cell formation play a significant role in ageing.

Referring back to the binding of dislocations by interstitials, that interaction which does occur would be expected to be changed once dislocation tangles have formed. The parent lattice will be severely distorted within the dense dislocation tangles which result when both metals are strained in their respective strain ageing ranges. Under these circumstances the lattice strain produced in titanium by interstitial oxygen - 12% in the "c" direction (Pearson, 1958) - should lead to a significantly greater stabilizing effect on these tangles than would be expected in zirconium, where the maximum strain is 4.4% (Lichter, 1960). That this is so is supported firstly by the more pronounced discontinuous yielding effects in titanium and secondly the differences observed in the stress relaxation behaviour of titanium and zirconium in their strain ageing temperature ranges. The more effective stabilization of dislocations in titanium would inhibit dislocation motion more effectively; also reloading to the initial stress value does not

appear to unlock stabilized dislocations, a different situation to that observed in zirconium (Wood, 1973). The stronger locking would also explain the generation of a room temperature yield point in high purity titanium after prior straining and ageing at 300°C, a phenomenon not observed in zirconium (see §3.1).

To obtain a peak in the $\Delta\sigma/\sigma$ versus temperature curve (figure 7) it would be expected that at the peak temperature, the diffusion of interstitials would be such that complete atmospheres would have time to form while thermal unpinning of dislocations would be maintained at a minimum. Pratt et al (1964) and Gupta and Weinig (1962) have both observed relaxation peaks in internal friction studies of titanium which they have shown are related to the diffusion of oxygen. The reported activation energies of 48000 and 45000 cal/gm. mole respectively are the same as reported for an oxygen peak in zirconium (Fuller, 1971). Ereemeev et al (1969) have found that the activation energies for bulk diffusion of nitrogen in titanium and zirconium are the same. Pemsler (1958) has reported an activation energy of 50800 cal/gm. mole for the bulk diffusion of oxygen in zirconium and Rosa (1970) has found an activation energy of 48600 cal/gm. mole for oxygen in titanium. Miller and

Browne (1968) have observed an internal friction peak in high purity titanium due to the reorientation of oxygen dipoles; the reported activation energy was 58000 ± 3000 cal./gm. mole.

From the foregoing it can be assumed that the diffusion rates of interstitials in the two metals are essentially the same; Fuller (1971) has determined the relaxation time for the oxygen peak in zirconium varies from 10000 seconds at 250°C to approximately 800 seconds at 300°C , 10 seconds at 350°C , and 0.1 seconds at 450°C . Assuming the same atom jump times in titanium, then for the ageing time used (1000 seconds) a peak in the ageing curve would be expected at about 300°C as was indeed the case. From this it must be concluded that interstitials also play an important role in the strain ageing behaviour of alpha-titanium even though they are not solely responsible for the phenomena observed.

5. CONCLUSIONS

Strain ageing effects in titanium have been reported in the literature for the last 20 years. To a large extent these observations have been made on impure titanium which shows significance differences to the performance of high purity material, the major one being the occurrence of a discontinuous yield point on initial strain, even at room temperature.

The present work revealed that to obtain a yield point in high purity material, a certain amount of prior strain is essential, and that further, significant ageing does not occur at temperatures much below 100°C. At the upper temperature limit of this work, 350°C, ageing effects are still quite marked.

The results obtained indicate that the mechanism of ageing is essentially the same as that proposed by Bedford (1970) for alpha-zirconium: dense dislocation tangles form during straining and ageing, with the consequence that strong dislocation-dislocation occurs. The formation of these tangles (cells) is not sufficient in itself to produce discontinuous yield points; many other metals exhibit cells without displaying evidence

of ageing. However, the diffusion of interstitial solute atoms to these tangles stabilizes them, effectively locking the dislocations in the cell walls.

Although an understanding of the basic mechanism responsible for strain ageing in high purity titanium has been achieved, many details still remain unresolved. The processes whereby cell formation occurs were not studied. Quenching of specimens immediately upon cessation of straining would enable the separation of those effects due only to straining and those due to ageing, hence providing more information relating to cell formation. Specimens quenched after varying ageing times would also yield information on the changes occurring during ageing. Long term stress relaxation experiments would also be useful in this regard, although the temperature stability of the apparatus was such as to limit the time interval over which these experiments could be conducted. The ascription of the role of stabilizing dislocations within cells to interstitials was deductive; however, the increasing sophistication of microanalysis techniques may enable more direct evidence to be obtained.

While the results of this work and those of Bedford (1970)

give a deeper insight into the spectrum of locking mechanisms which facilitate strain ageing in metals, a more complete understanding should be afforded if research is extended into three areas. Firstly, the effects of higher temperature should be examined, with particular attention paid to the modifications to dislocation structure wrought by recovery effects and their influence on ageing phenomena. Secondly, it is obvious from the literature that substitutional atoms greatly affect the behaviour of titanium; therefore, a study of the effects of composition on the ageing mechanism should yield fruitful results. Lastly, the influence of lattice parameter changes could be more fully evaluated by examining the ageing behaviour of both Hafnium and Scandium in detail.

BIBLIOGRAPHY

- ANTONY K.C. (1965), Paper presented to ASTM national meeting, Seattle, Washington, October.
- ARUNCHALAM V.S., PATTANAIK S., MONTEIRO S.M., REED-HILL R.E. (1972), *Met. Trans.*, 3, 1009.
- BAIRD J.D. (1971), *Met. Reviews*, 16, no. 149.
- BEDFORD A.J. (1970), Ph.D. thesis, Univ. of Adelaide.
- BEDFORD A.J., FULLER P.G., MILLER D.R.M. (1972), *J. Nuc. Materials*, 43, 164.
- BEDFORD A.J., MILLER D.R.M. (1970), *J.A.I.M.*, 15, 179.
- CHURCHMAN A.T. (1955), *Acta Met.*, 3, 22.
- CONRAD H., OKASAKI K., GADGIL V., JON M. (1972), *Electron Microscopy and Structure of Materials*, 438-469.
- CRUSSARD C. (1963), N.P.L. Symposium no. 15, 548.
- CUFF F.B., GRANT N.J. (1952), *Iron Age*, 170, (21), 134.
- EMEREEV V.S., IVANOV Yu.M., PANOV A.S. (1969), *Izvest. Akad. Nauk SSSR, Metally*, (4), 262.
- FIDLERIS V. (1968), *J. Nuc. Materials*, 26, 51.
- FULLER P.G. (1971), Ph.D. thesis, Univ. of Adelaide.
- GARDE A.M., SANTHANAM A.T., REED-HILL R.E. (1972), *Acta Met.*, 20, 215.
- GIFKINS R.C. (1970), *Optical Microscopy of Metals*.
- GUPTA D., WEINIG S. (1962), *Acta Met.*, 10, 292.
- HOLMES J.J. (1964), *J. Nuc. Materials*, 13, 137.

- HULL J., CONRAD H. (1967), Franklin Institute Report F-C1834.
- JONES R.L., CONRAD H. (1968), The Science, Technology and Applications of Titanium, 489.
- JONES R.L., CONRAD H. (1969), Trans. Met. Soc. AIME, 245, 779.
- KEELER J.H. (1955), Trans. A.S.M., 47, 157.
- KELLY P.M. (1972), Private communication.
- LICHTER B.D. (1960), Trans. AIME, 218, 1015.
- LUDWIK P. (1909), Elemente der Technologischem Mechanik, 32.
- LUSTER D.R., WENTZ W.W., KAUFMAN D.W. (1953), Materials and Methods, 37, 100.
- MILLER D.R., BROWNE K.M. (1968), The Science, Technology and Applications of Titanium, 401.
- NABARRO F.R.N. (1946), Proc. Phys. Soc., 58, 669.
- ORLOVA A., PAHUTOVA M., CADEK J., (1972), Phil. Mag., 25, 865.
- PARTRIDGE P.G. (1967), Met. Reviews, 12, no. 118
- PEARSON W.B. (1958), Handbook of Lattice Spacings and Structures of Metals, vol. 4.
- PEMSLER J.P. (1958), J. Electrochem. Soc., 105, 315.
- PRATT J.N., GRATINA W.J., CHAMBERS B. (1954), Acta Met., 2, 203.
- RAMASWAMI B., CRAIG G.B. (1967), Trans. Met. Soc. AIME, 218, 869.

- REED-HILL R.E., RAMACHANDRAN V., SANTHANAM A.T. (1969),
U.S.A.E.C. report ORO-AT-(40-1)-3262-10.
- RICE L., HINESLEY C.F., CONRAD H. (1971), *Metallography*,
4, 257.
- ROSA C.J. (1970), *Met. Trans.*, 1, (9), 2517.
- ROSI F.D., PERKINS F.C. (1953), *Trans. A.S.M.*, 45, 972.
- ROTSEY W.B. (1970), Private communication.
- ROTSEY W.B., SNOWDEN K.U. (1971), Private communication.
- SANTHANAM A.T., RAMACHANDRAN V., REED-HILL R.E. (1970),
Met. Trans., 1, 2593.
- SANTHANAM A.T., REED-HILL R.E. (1970), *Scripta Met.*, 4,
529.
- SMIALEK R.L., MITCHELL T.E. (1971), *Rev. Sci. Instruments*,
47, 890.
- STOKES G.K., KEOWN S.R., DYSON D.J. (1968), *J. App.*
Cryst., 1, 68.
- TRECO R.M. (1953), *Trans. A.S.M.*, 45, 872.
- TURNER N.G., ROBERTS W.T. (1968), *J. Less Common Metals*,
16, 37.
- TYSON W.R. (1967), *Can. Met. Qtly.*, 6, (4), 301.
- TYSON W.R. (1968), *The Science, technology and Applications*
of Titanium, 479.
- WOOD G.W. (1973), Ph.D. thesis, Univ. of Adelaide.

APPENDIX I

Preparation of 3 mm Disk Electron Microscopy Foils at
Sub-zero Temperatures

A technical note published in the *Journal of Scientific
Instruments*, 1972, 5, 984-5.

PREPARATION OF 3mm DISK ELECTRON MICROSCOPY FOLDS AT
SUB-ZERO TEMPERATURES.

A. S. Pearce and G. Wood

Materials Science Group, Chemical Engineering Department,
University of Adelaide, Australia.

MS received 30 May 1972.

ABSTRACT A polishing cell is described with accurate temperature control in the sub-zero range, for use with a helium-neon laser after the method of Smialek and Mitchell. The system ensures successful operation of the detector, which otherwise may be prevented by lack of temperature stability or icing in the light path.

1 INTRODUCTION

Automation of the 3mm disk technique has been traditionally accomplished with a light source directed at the disk, and a photoelectric cell to indicate the moment of perforation.

A suitable light source must of necessity be intense and well collimated, and the advent of low cost, low power lasers has provided an ideal source. Smialek and Mitchell (1971) have described a 3mm disk technique using

a laser, but their method, as described, was found to be unsuitable for use with electrolytes requiring sub-zero operating temperatures.

Modifications to the technique were required to eliminate two main problems: (1) the effects of polishing cell temperature fluctuations on photoelectric cell sensitivity; (2) formation of frost in the light path. The system adopted has overcome both these difficulties.

2 TEMPERATURE CONTROL

The normal method of standing the polishing cell in a freezing bath (methanol-solid CO_2) was discarded. Instead, the electrolyte (6% perchloric acid, 36% n-butanol, and 58% methanol) is cooled in a reservoir to below -60°C , again using a methanol-solid CO_2 coolant, and then pumped through the polishing cell and returned. A reservoir of 1 litre capacity, and a pumping rate of approximately 50ml min^{-1} were found to be suitable: with a faster flow of electrolyte the reservoir is difficult to maintain below -60°C .

The electrolyte was raised to the desired temperature of -35°C before flowing into the polishing cell by passing

it through a heater consisting of a stainless steel tube wound with kanthal and coupled to a Eurotherm stepless proportional controller. An iron-constantan thermocouple measured the electrolyte temperature immediately before the polishing cell.

3. POLISHING CELL

The polishing cell, shown in figure 1, was originally made from perspex, but has been replaced with Pyrex glass. The light guides are an integral part of the cell, and are paramount in overcoming the two aforementioned problems. Being good thermal insulators, they prevent ice forming in the light path and insulate the photoelectric detector from the polishing cell. Masking the outer surfaces of the light guides and most of the cell with PVC tape greatly reduces interference with the detector by stray light, though a window (shown as W in figure 1) is required so that the disk can be accurately aligned in the beam. Electrolyte flows upwards in the cell, and the flow rate used gives good uniform thinning of specimens.

4. ELECTRONICS

The alarm circuit diagram is shown in figure 2. The light dependent resistor is one arm of a bridge circuit which

is balanced with the disk in position but without the polishing current switched on. Output from the bridge goes to a high gain amplifier, with adjustable positive feedback. This enables the sensitivity of the amplifier to be set to filter out noise. Perforation of the disk switches off the polishing current via the relay and triggers an audible alarm.

5. SPECIMEN PREPARATION

3mm zirconium disks, about 0.5mm thick, were cut on a Servomet spark cutting machine, and profiled on both sides by jet machining. This dishing was done using an electrolyte of 5% perchloric acid in methanol at -50°C and a voltage of 200 volts DC. Titanium disks were profiled chemically using the method of Rice et al (1971). Specimens were coated with Lacomit stopping off compound around the edges, gripped in modified tweezers, and placed in the laser beam (model 410, Metrologic Instruments, Bellmawr, NJ 08030). The polishing power supply was then switched on**; immediately the alarm sounded the specimen was removed from the cell, washed in clean methanol and dried. Delays in washing in excess of two seconds will result in dirty specimens.

The perforations averaged approximately 100 microns

in diameter, with adequate areas transparent to 100kV electrons. Although the apparatus has only been used for Zr and Ti, it should be suitable for any material requiring sub-zero polishing conditions.

ACKNOWLEDGMENTS

The authors wish to thank Mr. B. Ide for help with the cell, pump and heater, and Mr. V. Kendall for the electronics. One of the authors (ASP) gratefully acknowledges the support of the Australian Research Grants Committee.

REFERENCES

Rice L, Hinesly C P and Conrad H 1971 METALLOGRAPHY

4 257-68

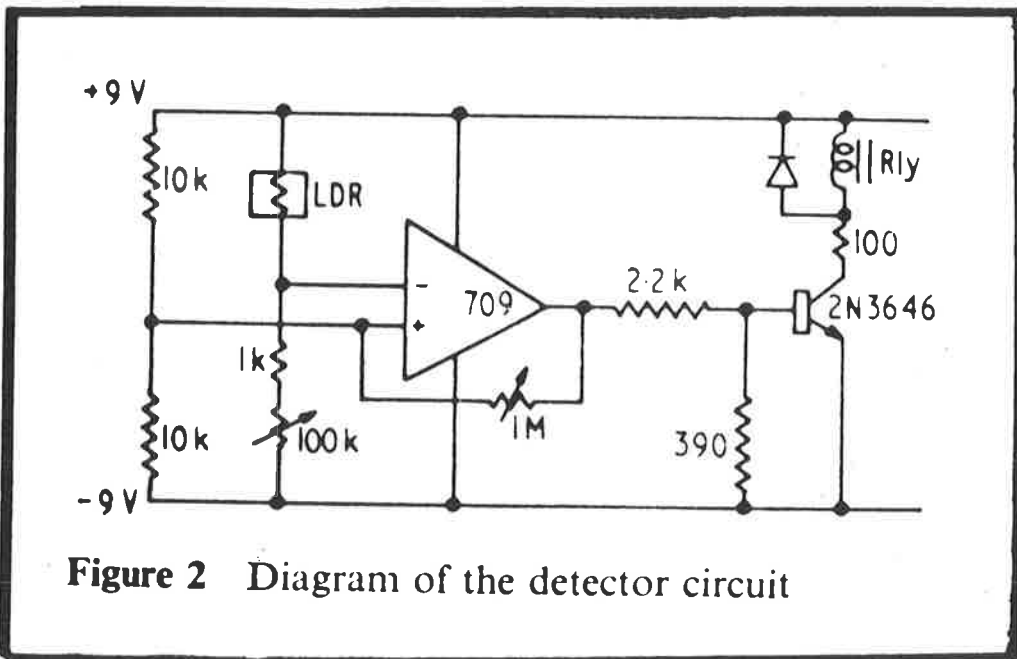
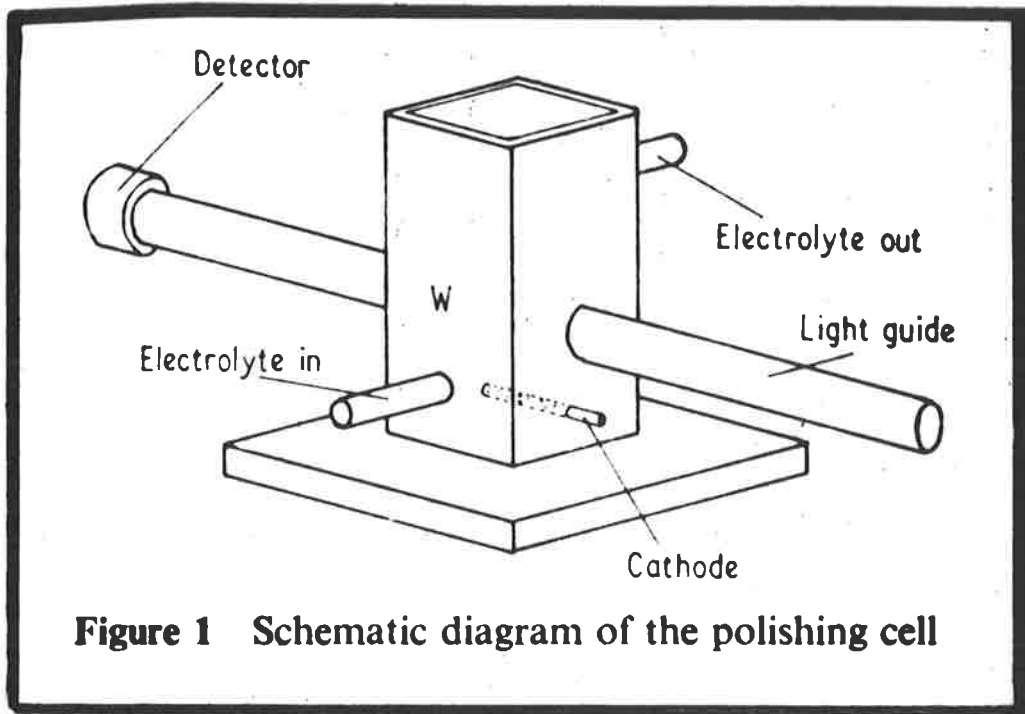
Smialek B L and Mitchell T E 1971 REV. SCI. INSTRUM.

42 890-1

** 20.5 V was used for Zr and 10.5 V for Ti.

Journal of Physics E: Scientific Instruments 1972 Volume 5

Printed in Great Britain © 1972



APPENDIX II

Automatic Plotting of Stereographic Projections.

AUTOMATIC PLOTTING OF STEREOGRAPHIC PROJECTIONS1. INTRODUCTION

The value of stereographic projections has long been recognised by crystallographers. While there are many "standard" projections available in the literature, projections other than these standards are often preferred. Manual construction of projections tends to be time consuming and tedious, and to this end the following program has been written for use with the CDC 6400 computer with Calcomp 10" and 30" plotters.

2. SUMMARY

A fortran program has been written to produce stereographic projections, both planar and directional, of any orientation for any crystal system which can be described by three noncoplanar axes and three inter-axial angles. It is summarised in terms of planar projections; plotting of directional projections is completely analogous. It is also assumed that the concepts of stereographic sphere and projection are understood.

To facilitate the actual mechanics of plotting the projection three reference axes (plane normals) are required, one of which is the normal to the

projection plane. Once the point to be plotted has been chosen the angles which the plane normal in question make with each of the three reference axes are calculated. It is then a relatively simple trigonometric operation to plot the point. The trigonometry is considerably simplified if the reference axes are mutually perpendicular. However, for many non-standard projections, particularly in non-cubic systems, three mutually perpendicular plane normals may not be known. This deficiency can be easily overcome using a basic property of vectors, namely, that the cross product of two vectors will yield a third perpendicular to the first two. If vectors #1 and #3 are then crossed, a fourth vector will result that is perpendicular to these, thus producing three vectors, #1, #3, and #4, which are mutually perpendicular.

The program is written to give the operator options as to the size of the plot, which plotter (10" or 30") is used, whether it is of planes or projections, the order of planes or directions considered, and whether or not a print out of point co-ordinates is required. If these options are not exercised the program assigns default values to enable it to run.

3. PROGRAM DETAILS

3.1 Language: FORTRAN IV

3.2 Data Input:

- (i) Radius of plot and choice of plotter.
- (ii) Number of projections to be plotted.
- (iii) Lattice parameters $a, b, c, \alpha, \beta, \gamma$.
- (iv) Program controls. These limit the order of planes plotted and whether planes and directions are considered.
- (v) Pole of the projection and two mutually perpendicular reference planes. If the latter poles are not given, the computer generates its own.

3.3 Calculations.

Using the given lattice parameters those of the reciprocal lattice are calculated from the following:-

$$V = a.b.c. (\cos^2 \alpha + \cos^2 \beta + \cos^2 \gamma - 2.\cos\alpha.\cos\beta.\cos\gamma)^{\frac{1}{2}}$$

where V is the unit cell volume.

Then

$$a^* = \frac{b.c.\sin\alpha}{V}$$

and

$$\cos(\alpha)^* = \frac{\cos\beta\cos\gamma - \cos\alpha}{\sin\beta.\sin\gamma}$$

b^* , etc., are calculated cyclicly.

If the two reference poles are not supplied they are generated using the following relations:-

Consider two sets of planes (i.e.

vectors in reciprocal space) $(u_i v_i w_i)$ and $(u_j v_j w_j)$, then because of the relationships between real and reciprocal space,

$$(u_i v_i w_i) \times (u_j v_j w_j) = [UVW]$$

where UVW is a vector in real space and is, of course, perpendicular to both $(u_i v_i w_i)$ and $(u_j v_j w_j)$:

$$U = v_j w_i - w_j v_i$$

$$V = w_j u_i - u_j w_i$$

$$W = u_j v_i - v_j u_i$$

$[UVW]$ is then converted to a vector (uvw) in reciprocal space as follows:

$$u = U.a^2 + V.a.b.\cos\gamma + W.c.a.\cos\beta$$

$$v = U.a.b.\cos\gamma + V.b^2 + W.b.c.\cos\alpha$$

$$w = U.c.a.\cos\beta + V.b.c.\cos\alpha + W.c^2$$

The actual procedure is then:

$$(u_2 v_2 w_2) \text{ is given by } (100) \times (u_1 v_1 w_1)^{**}$$

$$(u_3 v_3 w_3) \text{ is given by } (u_1 v_1 w_1) \times (u_2 v_2 w_2)$$

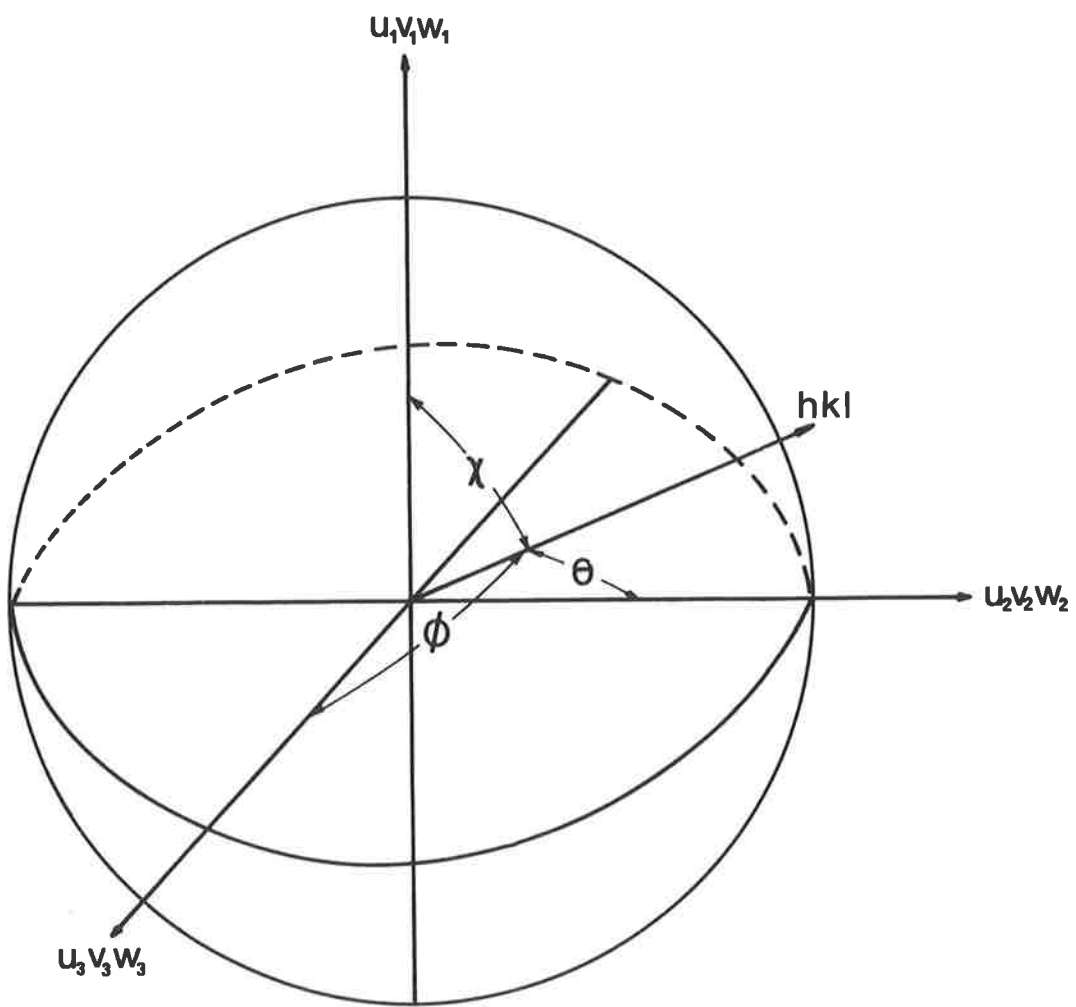
** if $(u_1 v_1 w_1) = (100)$, then it is crossed with (111)

In this way three mutually perpendicular axes are produced.

The Miller index triplets are then generated and tested for a common factor; if none exists the angles χ , ϕ , and θ are calculated.

From these angles, the x and y

Figure 1: The stereographic sphere



co-ordinates of each point is calculated (poles on the back hemisphere are omitted by ignoring those poles with $\chi > 90^\circ$).

The expressions used are:-

$$x = -R \cdot \cos\phi \cdot \tan\left(\frac{\chi}{2}\right) \cdot (\cos^2\phi + \cos^2\theta)^{-\frac{1}{2}}$$

$$y = R \cdot \cos\theta \cdot \tan\left(\frac{\chi}{2}\right) \cdot (\cos^2\phi + \cos^2\theta)^{-\frac{1}{2}}$$

The triplets are generated until $d_{uvw} < d_{limit}$, and are stored along with the plot co-ordinates and interplanar spacings until calculation is complete. The stereographic projection is then plotted.

3.4 Default Values.

Input data requirements have been given in 3.2. However, of these only the lattice parameters are essential for the program to run. The other parameters have default values assigned according to the following table:-

<u>Parameter</u>	<u>Read Value</u>	<u>Default Value</u>
Plot radius	0 cms.	5 cms.
No. of plots	0	1
Planes or dirns.	≠ D	P
Limiting order of points plotted	(0,0,0)	(2,2,2)
Proj. plane	(0,0,0)	(0,0,1)

If only the lattice parameters are supplied in the data list the result will be a (001) projection of plane normals,

10 cms. in diameter, including planes up to $d_{(uvw)} \geq d_{(222)}$, plotted on the 10" plotter.

4. CONCLUSION

The program has been used successfully to produce several projections for the hexagonal system, $c/a = 1.59$, as well as for cubic and orthorhombic systems. Two examples of the plots obtained are shown in figures 2 and 3. A program listing is also given.

Figure 2: The (111) projection for planes in titanium - $c/a = 1.59$

(111) Projection for Planes, Hexagonal - $c:a=1.59$

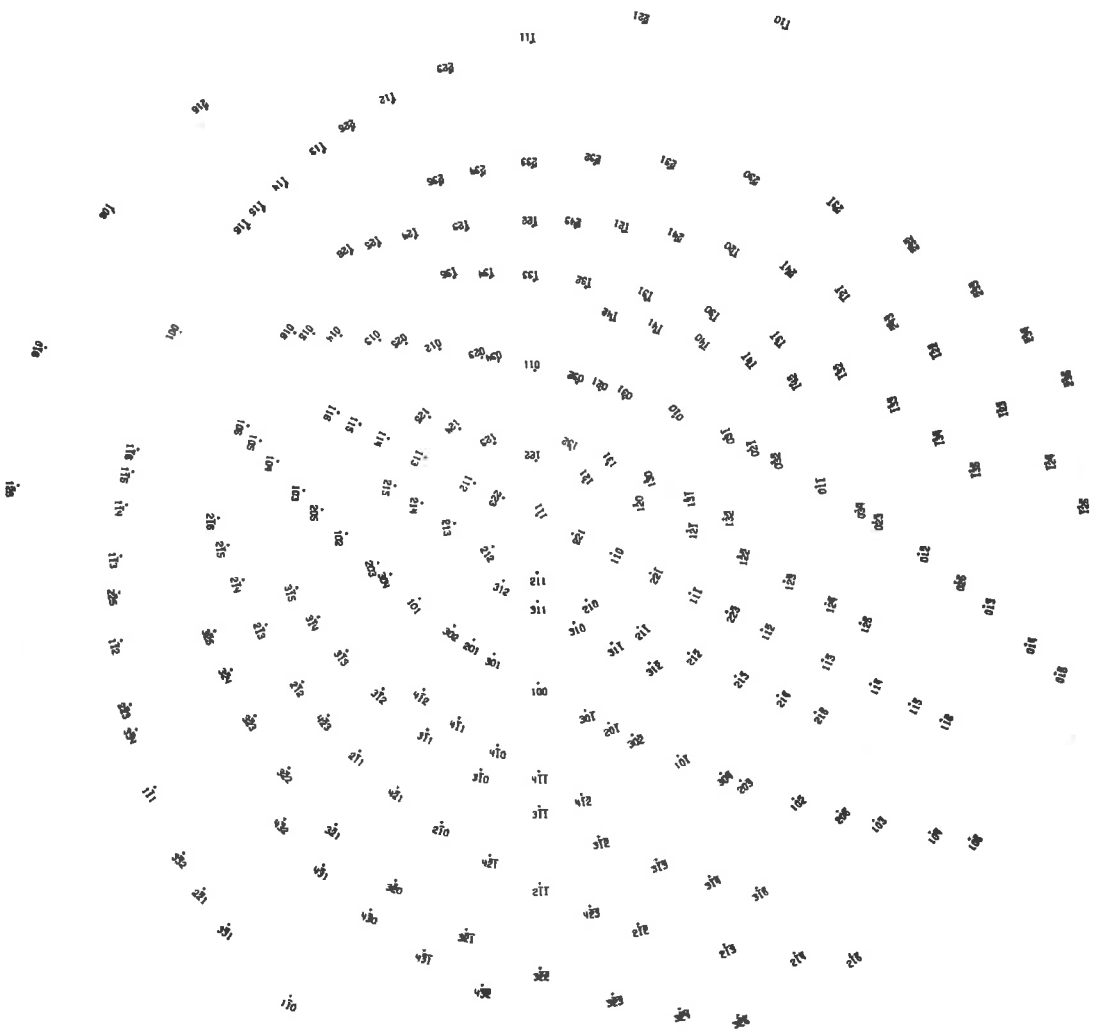
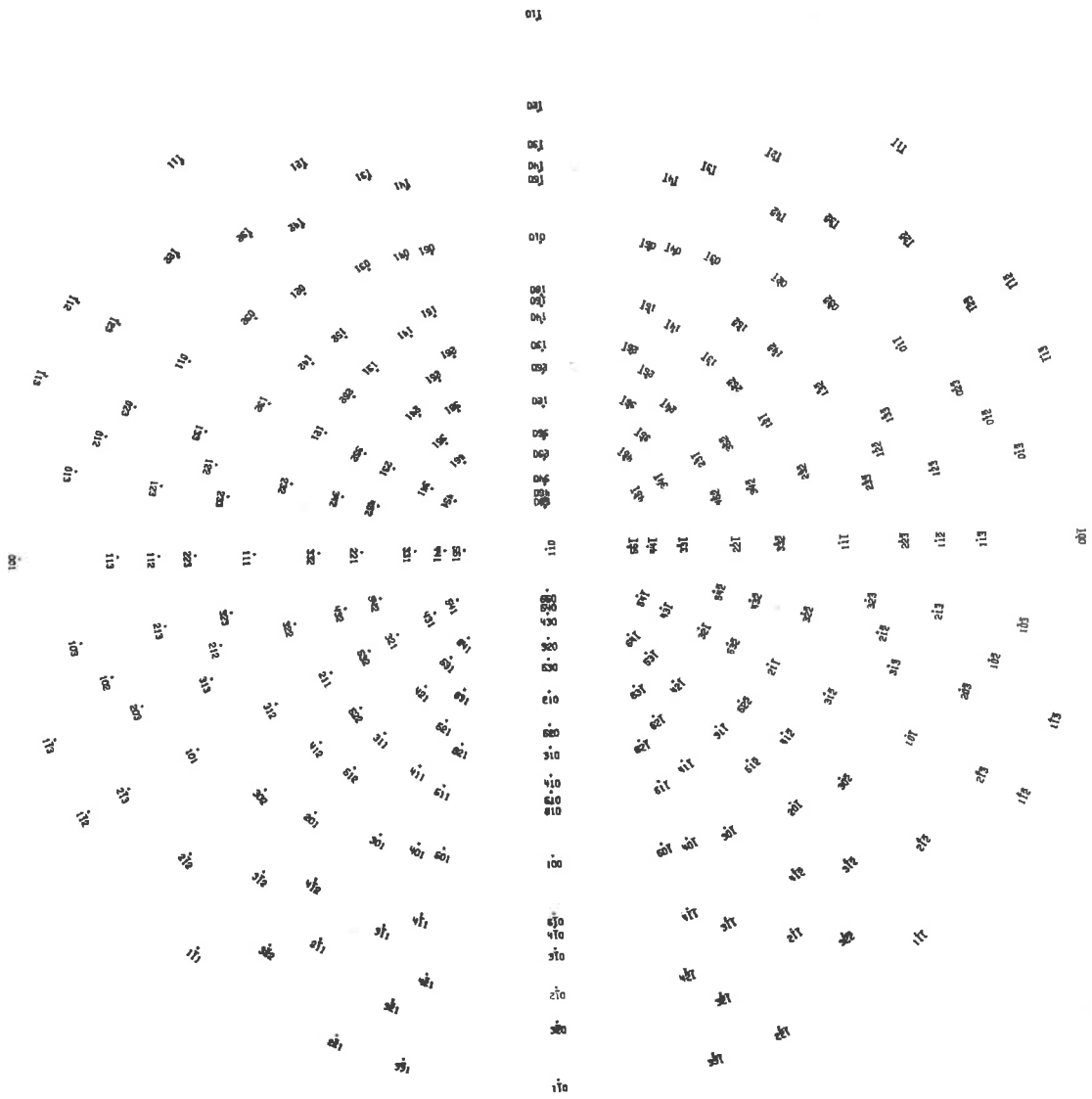


Figure 3: The $[110]$ projection for directions
in titanium - $c/a = 1.59$

[110] Projection for Directions - Hexagonal, $c:a = 1.59$



```

PROGRAM STEREO(INPUT,OUTPUT)
INTEGER H(400), HH, F
REAL LIMIT, LIMH, LIMK, LIML
DIMENSION X(400),Y(400),K(400),L(400),IC(5)
LOGICAL HLIM,KLIM,EXC
DATA PI,IC/3.1415927,2,3,5,7,11/
COMMON/ANG/ A,B,C,COSALP,COSBET,COSGAM,HH,KK,LL
COMMON/CONVERT/ASTR,BSTR,CSTR,ALPSTR,BETSTR,GAMSTR
ICONT = 0

```

```

*
* READ RADIUS (IN CMS.) AND PLOTTER
* CONTROL (10 OR 30 INCH).
*

```

```

READ 205, R,ITEN
IF(R.LE.0.) R = 5.
IF(R.LT.12.5.A.ITEN.EQ.0)202,203
202 CALL PLOT 10 (7HNNHDEYCU,7)
GO TO 204
203 CALL PLOT 30 (7HNNHDEYCU,7)
204 CALL PAUPL0T(18HBLANK PAPER PLEASE,18)
205 FORMAT (F5,I1)
R=R*0.393701
XR = R
YR = R

```

```

*
* READ NO. OF PROJECTIONS TO BE PLOTTED
* AND PRINT SUPPRESSION IF REQUIRED
*

```

```

READ 14, NP,IPRINT
14 FORMAT (2I3)
IF(NP.GT.0) GO TO 207
NP = 1
207 PXM = 3*(R+5)*NP
CALL XLIMIT (PXM)

```

```

*
* READ LATTICE PARAMETERS. INTERAXIAL ANGLES
* ARE IN DEGREES.
*

```

```

12 READ 1, A,B,C,ALP,BET,GAM
1 FORMAT (3F10.5,3F10.3)
IF(A.LE.0..0.B.LE.0..0.C.LE.0.) GO TO 200
IF(ALP.LE.0..0.BET.LE.0..0.GAM.LE.0.) GO TO 200
ALP = ALP*PI/180.
BET = BET*PI/180.
GAM = GAM*PI/180.
EXC = .F.
21 COSALP = COS(ALP) $ SINALP = SIN(ALP)
COSBET = COS(BET) $ SINBET = SIN(BET)
COSGAM = COS(GAM) $ SINGAM = SIN(GAM)
IF(EXC)GO TO 37

```



```

SQT = 1.-COSALP**2-COSBET**2-COSGAM**2
1   + 2.*COSALP*COSBET*COSGAM
RECVOL = A*B*C*(SQRT(SQT))
ASTR = B*C*SINALP/RECVOL
BSTR = C*A*SINBET/RECVOL
CSTR = A*B*SINGAM/RECVOL
CASTR = (COSBET*COSGAM-COSALP)/SINBET/SINGAM
CBSTR = (COSGAM*COSALP-COSBET)/SINGAM/SINALP
CGSTR = (COSALP*COSBET-COSGAM)/SINALP/SINBET

```

```

*
* READ LIMITING INDICES AND WHETHER PLANAR
* OR DIRECTIONAL.
*

```

```

READ 2, LIMH,LIMK,LIML,OPT
2  FORMAT (3F3,A1,F5)
IF (LIMH.NE.0.0.LIMK.NE.0.0.LIML.NE.0) GO TO 250
LIMH = LIMK = LIML = 2
250 CONTINUE
ALPSTR = ACOS(CASTR)
BETSTR = ACOS(CBSTR)
GAMSTR = ACOS(CGSTR)
IF(OPT.EQ.1HD)GO TO 37
AR = A $ BR = B $ CR = C
APR = ALP $ BTR = BET $ GMR = GAM
A = ASTR
B = BSTR
C = CSTR
ALP = ALPSTR
BET = BETSTR
GAM = GAMSTR
ASTR = AR $ BSTR = BR $ CSTR = CR
ALPSTR = APR $ BETSTR = BTR $ GAMSTR = GMR
EXC = .T.
GO TO 21

```

```

37 CONTINUE

```

```

*
* READ PROJECTION POLE AND REFERENCE POLES
*

```

```

READ 3, U1,V1,W1,U2,V2,W2,U3,V3,W3
3  FORMAT (9F5)
IF(U1.NE.0.0.V1.NE.0.0.W1.NE.0.0) GO TO 206
U1=V1=0. $ W1=1.
206 IREF = KREF = 1
IF(U2.EQ.0.0.A.V2.EQ.0.0.A.W2.EQ.0.0) IREF = 0
IF(U3.EQ.0.0.A.V3.EQ.0.0.A.W3.EQ.0.0) KREF = 0
IF(IREF.NE.0.A.KREF.NE.0) GO TO 41

```

```

*
* THIS SECTION GENERATES THE REFERENCE
* POLES IF NECESSARY.
*

```

```

IF(JREF.EQ.0.A.KREF.EQ.0) GO TO 42
IF(KREF.EQ.0) GO TO 43
U2 = U3 $ V2 = V3 $ W2 = W3
GO TO 43
42 IF(U1.EQ.1..A.V1.EQ.0..A.W1.EQ.0.)251,252
251 TV = TU = TW = 1.
GO TO 420
252 TU = 1.
TV = TW = 0.
420 UT = TV*W1 - TW*V1
VT = TW*U1 - TU*W1
WT = TU*V1 - TV*U1
CALL AXCHAN (UT,VT,WT,U2,V2,W2)
43 UT = V2*W1 - W2*V1
VT = W2*U1 - W1*U2
WT = U2*V1 - U1*V2
CALL AXCHAN (UT,VT,WT,U3,V3,W3)
*
PRINT 16
PRINT 13, A,B,C,ALP,BET,GAM
PRINT 13, U1,V1,W1,U2,V2,W2,U3,V3,W3
13 FORMAT (10X,9F10.4)
*
41 CONTINUE
PRINT 16
16 FORMAT (1H1)
LIMIT = SPACE(LIMH,LIMK,LIML)
SPAXIS = SPACE(U1,V1,W1)
SPX = SPACE(U2,V2,W2)
SPY = SPACE(U3,V3,W3)
HH = KK = LL = -1
NO=0
INCH = INCK = INCL = 1
4 HH = HH + INCH
5 KK = KK + INCK
6 LL = LL + INCL
IF(HH.EQ.0.A.KK.EQ.0.A.LL.EQ.0)GO TO 6
RH = HH $ RK = KK $ RL = LL
PS = SPACE(RH,RK,RL)
IF(PS.LT.LIMIT)GO TO 7
COSPHI = ANGLE(U1,V1,W1,PS,SPAXIS)
IF(COSPHI.LT.-1.E-03)GOTO6
*
* INDICES WITH A COMMON FACTOR ARE ELIMINATED.
*
DO 20 F=1,5
TN = FACTOR(HH,IC(F))
RH = TN - HH
TN = FACTOR(KK,IC(F))
RK = TN - KK

```

```

TN = FACTOR(LL,IC(F))
RL = TN - LL
IF(RH.EQ.0..A.RK.EQ.0..A.RL.EQ.0.)GOTO6
20 CONTINUE

*
NO = NO + 1
H(NO) = HH
K(NO) = KK
L(NO) = LL
COSPSI = ANGLE(U2,V2,W2,PS,SPX)
COSTHI = ANGLE(U3,V3,W3,PS,SPY)
PO = ACOS(COSPHI)
PO2 = PO/2.
TMP = R*TAN(PO2)/(SQRT(COSPSI**2 + COSTHI**2))
X(NO) = -COSPSI*TMP
Y(NO) = COSTHI*TMP
IF(IPRINT.NE.0) GO TO 15
PRINT 95, H(NO),K(NO),L(NO),PS,H(NO),K(NO),L(NO),
1 X(NO),Y(NO)
95 FORMAT (10X,3I3,F20.10,40X,3I3,2F10.5)
15 KLIM = .F.
HLIM = .F.
GO TO 6
7 INCL = -INCL & LL = -INCL
IF(INCL.LT.0)61,8
61 LL = 0
GO TO 6
8 CONTINUE
IF(KLIM)GO TO 9
KLIM = .T.
GO TO 5
9 INCK = -INCK
KK = -INCK
KLIM = .F.
IF(INCK.LT.0)81,82
81 KK = 0
GO TO 8
82 IF(HLIM)GO TO 10
HLIM = .T.
GO TO 4
10 IF(INCH.LT.0)GO TO 11
INCH = -INCH
HH = 0
HLIM = .F.
GO TO 4
11 CONTINUE
ER = -.0001
SYM = 1H+
CALL PLOT (XR,YR,-3)
XR = 2*(R+2)

```

```

YR = 0
ICONT = ICONT + 1
DO 60 J = 1,NO
XM = ABS(X(J)) $ YM = ABS(Y(J))
G = XM**2 + YM**2 $ GG = SQRT(G)
IF(GG.NE.0.) GO TO 46
THETA = 0. $ GO TO 47
46 ALF = YM/GG
THETA = ASIN(ALF) + PI/2
47 CONTINUE
IF(X(J).LT.ER.A.Y(J).GE.ER) THETA = 2.*PI - THETA
IF(X(J).LT.ER.A.Y(J).LT.ER) THETA = THETA + PI
IF(X(J).GE.ER.A.Y(J).LT.ER) THETA = PI - THETA
SLH = SLK = SLL = 1H
IF(H(J).GE.0)GOTO70
H(J) = -H(J)
SLH = 1H-
70 IF(K(J).GE.0)GOTO71
K(J) = -K(J)
SLK = 1H-
71 IF(L(J).GE.0)GOTO72
L(J) = -L(J)
SLL = 1H-
72 CONTINUE
ENCODE(3,73,SLASH)SLH,SLK,SLL
73 FORMAT(A1,A1,A1)
ENCODE(3,74,ICHAR)H(J),K(J),L(J)
74 FORMAT(I1,I1,I1)
CALL SYMBOL(X(J),Y(J),.04,SYM,0.,1)
ALFA = THETA + .7854
XC = .0781*COS(ALFA)
YC = .0781*SIN(ALFA)
XJ = X(J) - XC
YJ = Y(J) - YC
THEDA = THETA*180./PI
CALL SYMBOL(XJ,YJ,.07,SLASH,THEDA,3)
ALFA = THETA + 1.1071
XC = .1253*COS(ALFA)
YC = .1253*SIN(ALFA)
XJ = X(J) - XC
YJ = Y(J) - YC
60 CALL SYMBOL(XJ,YJ,.07,ICHAR,THEDA,3)
IF(ICONT.LT.NP) GO TO 12
CALL PLOT(0.,0.,-3)
GO TO 501
200 PRINT 201
201 FORMAT(10X,*LATTICE PARAMETER HAS BEEN READ*,
1 * AS LESS THAN OR EQUAL TO ZERO. JOB ABORTED.*)
501 STOP
END

```

```
FUNCTION SPACE(U,V,W)
COMMON/ANG/ A,B,C,COSALP,COSBET,COSGAM,HH,KK,LL
SQSP = (U*A)**2+(V*B)**2+(W*C)**2
SQSR = 2.*U*V*A*B*COSGAM
SQSQ = 2.*V*W*B*C*COSALP
SQST = 2.*W*U*C*A*COSBET
SQDT = SQSP+SQSR+SQSQ+SQST
SPACE = 1./SQRT(SQDT)
RETURN
END
```

```
FUNCTION FACTOR(I,M)
  RG = M
  NI = I/RG
  FACTOR = NI*RG
  RETURN
END
```

```
FUNCTION ANGLE(U,V,W,SPC,RSP)
INTEGER HH
COMMON/ANG/ A,B,C,COSALP,COSBET,COSGAM,HH,KK,LL
T1 = HH*U*A*A+KK*V*B*B+LL*W*C*C
T2 = (KK*W+LL*V)*B*C*COSALP
T3 = (HH*W+LL*U)*A*C*COSBET
T4 = (HH*V+KK*U)*A*B*COSGAM
ANGLE = SPC*RSP*(T1+T2+T3+T4)
RETURN
END
```

```
SUBROUTINE AXCHAN (RH,RK,RL,U,V,W)
COMMON/CONVERT/ASTR,BSTR,CSTR,ALPSTR,BETSTR,GAMSTR
T1 = ASTR*BSTR*COS(GAMSTR)
T2 = BSTR*CSTR*COS(ALPSTR)
T3 = CSTR*ASTR*COS(BETSTR)
U = RH*ASTR*ASTR + RK*T1 + RL*T3
V = RH*T1 + RK*BSTR*BSTR + RL*T2
W = RH*T3 + RK*T2 + RL*CSTR*CSTR
RETURN
END
```


APPENDIX III

Analysis of the burgers vectors of dislocations in
alpha-titanium.

The consistently indexed solutions of these two diffraction patterns are shown in figure 3. The operative reflections were $(1\bar{1}\bar{2})$ which corresponds to $g = [1\bar{1}\bar{1}]$, and $(\bar{1}13)$ which corresponds to $g = [\bar{1}13]$. The burgers vector, which must be perpendicular to both these, is therefore $[110]$ (or $[11\bar{2}0]$ in Miller-Bravais notation),

Figure 1: That section of the Kikuchi map
representing the tilting experiment.

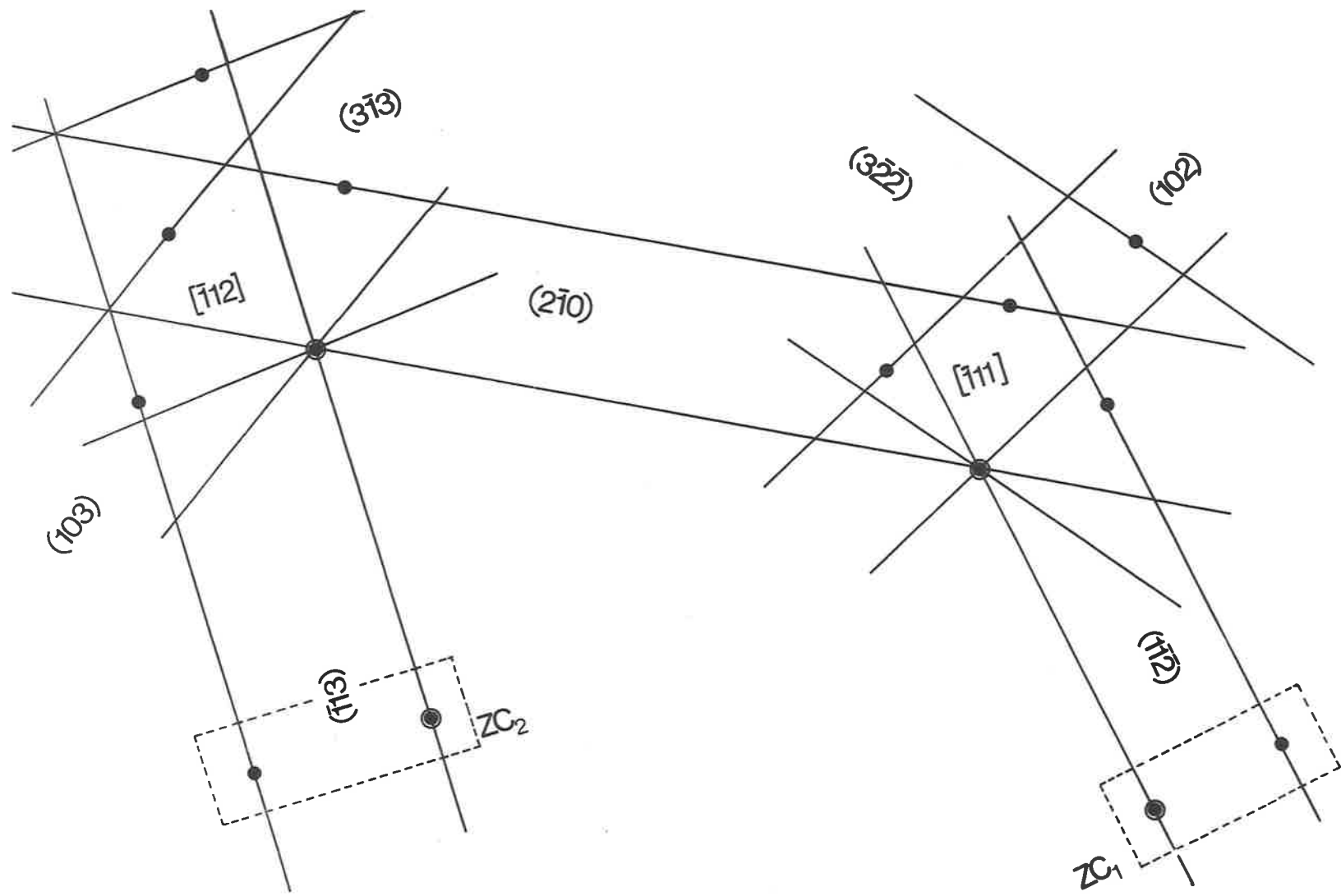


Figure 2: Schematic representations of the two Kikuchi poles used to identify the operating reflections.

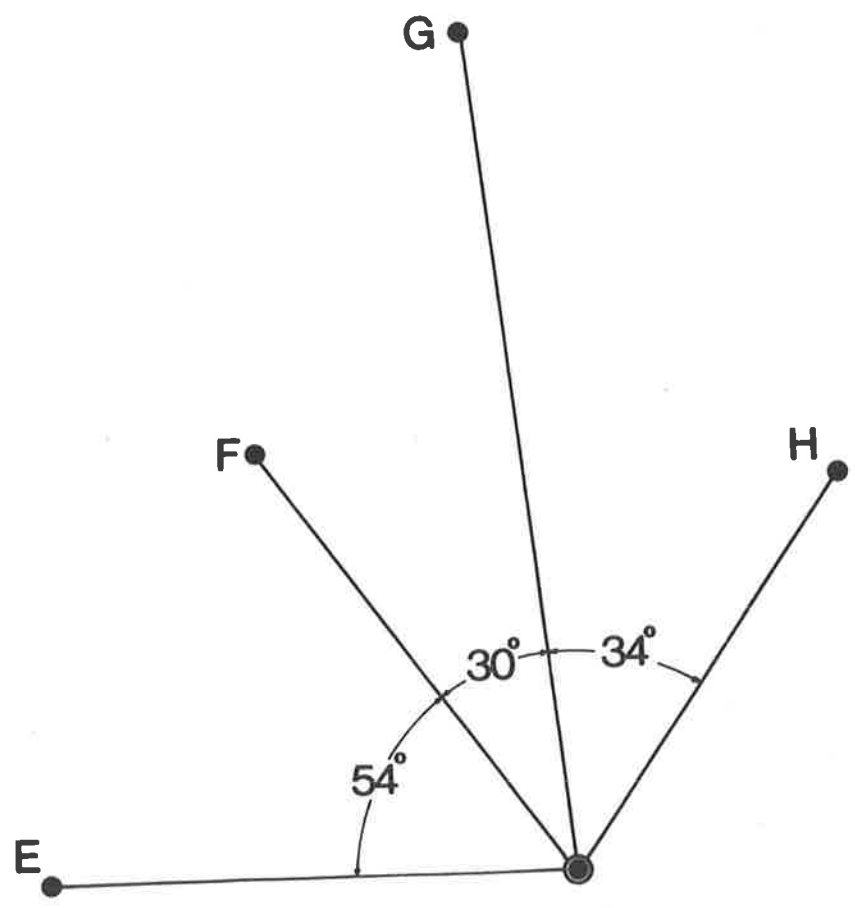
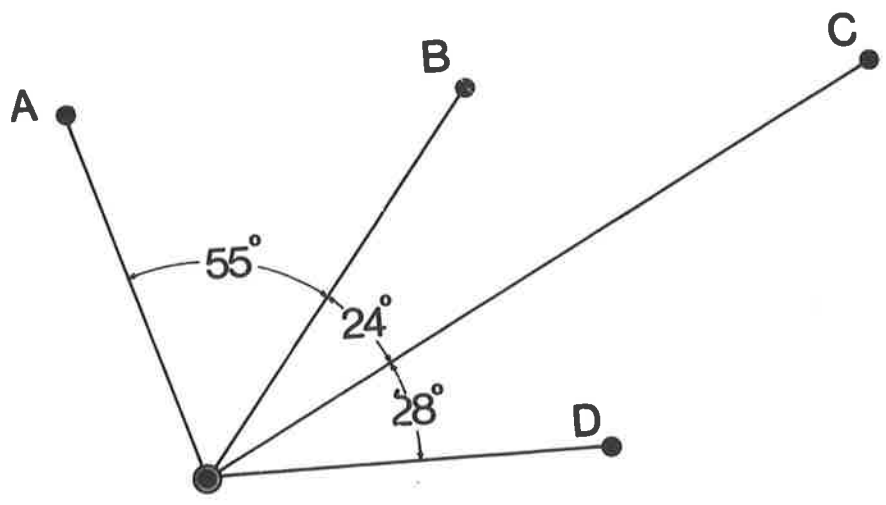
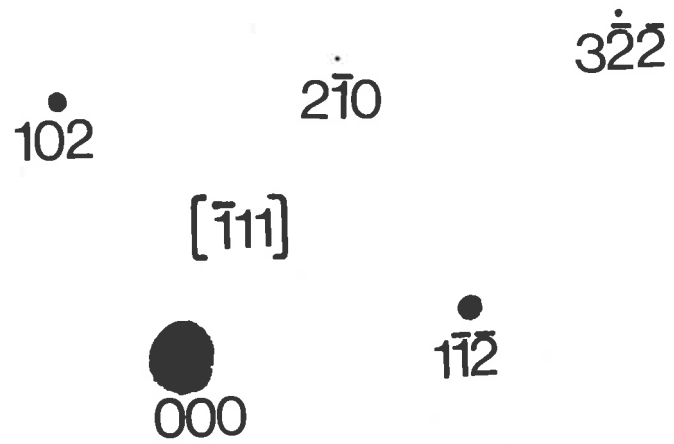
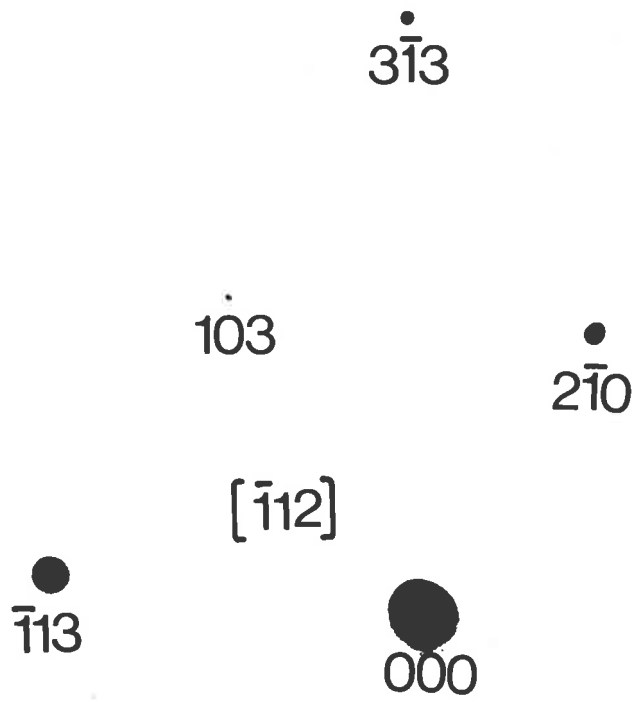


Figure 3: Solutions of the two electron
diffraction patterns.



(a)



(b)


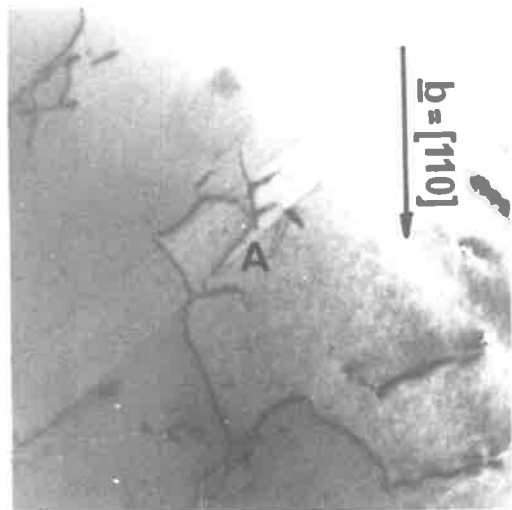
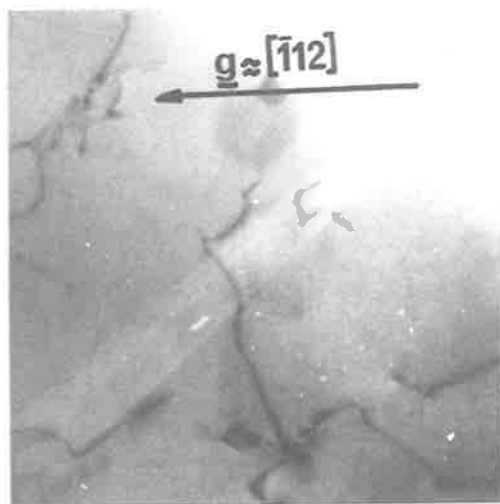


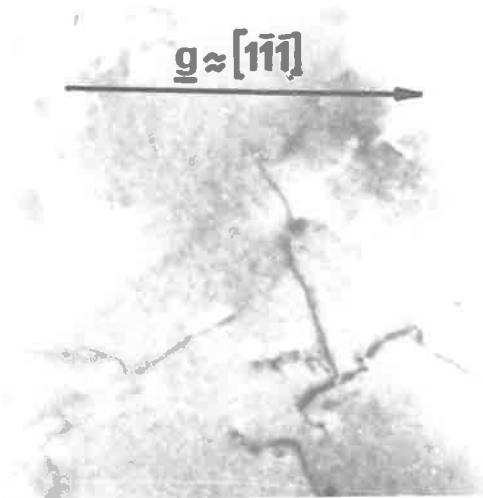
Figure 4: Showing the conditions of zero contrast
for dislocation A.



(a)



(b)



(c)